Please cite this article in press as: Hillen et al., Targeting white matter astrocytes with a *Gfap*-disruptive Cas9 nuclease benefits a murine model of Alexander disease, Molecular Therapy (2026), https://doi.org/10.1016/j.ymthe.2026.09.019

**Molecular Therapy**
Original Article

# Targeting white matter astrocytes with a *Gfap*-disruptive Cas9 nuclease benefits a murine model of Alexander disease

Anne E.J. Hillen,[1] Irene Capuano,[1] Barbara Gega,[2] Rossana Norata,[3] Margaux Mombled,[4,5] Ilaria Laface,[1] Giada Zambonini,[1] Andrea Lomagno,[2] Marine Rouillon,[4,5] Serena G. Giannelli,[6] Fabrizio Benedicenti,[2] Francesco Gazzo,[2] Sergio Arévalo,[2] Giulio Spinozzi,[2] Francesca Sanvito,[3,7] Mario Amendola,[4,5,8] Vania Broccoli,[6,9] Eugenio Montini,[2] Angela Gritti,[1,10] and Vasco Meneghini[1,10]

[1]San Raffaele Telethon Institute for Gene Therapy (SR-Tiget), IRCCS San Raffaele Scientific Institute, Gene/Neural stem cell therapy for lysosomal storage diseases, 20132 Milan, Italy; [2]San Raffaele Telethon Institute for Gene Therapy (SR-Tiget), IRCCS San Raffaele Scientific Institute, Safety of gene therapy and insertional mutagenesis research, 20132 Milan, Italy; [3]San Raffaele Telethon Institute for Gene Therapy (SR-Tiget), IRCCS San Raffaele Scientific Institute, SR-TIGET GLP Test Facility, 20132 Milan, Italy; [4]Genethon, 91042 Evry, France; [5]Université Paris-Saclay, University of Evry, Inserm, Integrare Research Unit UMR_S951, 91042 Evry-Courcouronnes, France; [6]Division of Neuroscience, IRCCS San Raffaele Scientific Institute, Stem Cell and Neurogenesis Unit, 20132 Milan, Italy; [7]Division of Experimental Oncology, IRCCS San Raffaele Scientific Institute, Pathology Unit, 20132 Milan, Italy; [8]Department of Clinical and Experimental Medicine, University of Foggia, 71122 Foggia, Italy; [9]CNR Institute of Neuroscience, 20129 Milan, Italy; [10]Vita-Salute San Raffaele University (UniSR), 20132 Milan, Italy

**Astrocytes are intriguing therapeutic targets due to their crucial role in initiating and promoting demyelination in the central nervous system. By efficient on-target editing, we can permanently disrupt detrimental genes and restore normal physiological processes. Here, we have optimized an adeno-associated viral (AAV) platform to deliver the CRISPR-Cas9 system to white matter astrocytes. A single neonatal intra-CSF administration of an all-in-one AAV-DJ8 vector expressing the *Staphylococcus aureus* Cas9 enzyme under an astrocyte-specific promoter resulted in effective downregulation of glial fibrillary acidic protein (GFAP), which is responsible for the primary astrocytic dysfunctions in Alexander disease (AxD), a fatal leukodystrophy. This treatment achieved an editing rate of up to 32% in *Gfap*$^{+/R76H}$ mice, leading to decreased gliosis and reduced formation of Rosenthal fibers, an AxD pathological hallmark. The integration of the AAV vector occurred at low abundance in the host genome, showed a positive correlation with transduction and gene editing efficiencies, and did not cause tumorigenic events. Overall, this study demonstrates the feasibility of gene editing strategies and paves the way for therapies treating AxD and other demyelinating disorders.**

## INTRODUCTION

Astrocytes are the most abundant cells in the mammalian brain, making up 20%–40% of neural cell populations.[1] They play a critical role in brain development and maintenance of homeostasis in the central nervous system (CNS), in part by promoting myelination in the fetal brain and sustaining myelin integrity in the adult brain. Astrocytes influence the dynamics of the extracellular matrix and secrete factors that affect the proliferation and maturation rate of oligodendrocyte progenitor cells (OPCs) and drive myelination in mature oligodendrocytes.[2,3] Recent interest has focused on their role in neurodegeneration, particularly in demyelinating disorders, leading to therapeutic strategies that target astrocytes to prevent cell death and restore the normal functions of neurons and oligodendrocytes.[4,5]

Alexander disease (AxD; OMIM: 203450) is a rare, progressive leukodystrophy caused by autosomal dominant mutations in the gene encoding glial fibrillary acidic protein (*GFAP*), the major intermediate filament protein of astrocytes.[6,7] Most cases arise *de novo*, though inherited forms are reported.[8] More than 100 pathogenic GFAP variants have been identified, mainly missense mutations in the GFAP-α isoform, with hotspots at residues R79 and R239.[9,10] These mutations cause toxic gain of function, impairing filament assembly and protein turnover and leading to the accumulation of Rosenthal fibers (RFs), the pathological hallmark of AxD.[11,12] Elevated GFAP and RFs drive astrocytic dysfunction,[13–15] including impaired proteasomal activity, oxidative stress, disrupted vesicle trafficking, altered metabolism, senescence, and reactive astrogliosis.[16–22] Dysfunctional astrocytes ultimately affect neurons, promote microglia activation,

Received 23 July 2025; accepted 15 September 2026;
https://doi.org/10.1016/j.ymthe.2026.09.019.

**Correspondence:** Angela Gritti, San Raffaele Telethon Institute for Gene Therapy (SR-Tiget), IRCCS San Raffaele Scientific Institute, Gene/Neural stem cell therapy for lysosomal storage diseases, 20132 Milan, Italy.
**E-mail:** gritti.angela@hsr.it
**Correspondence:** Vasco Meneghini, San Raffaele Telethon Institute for Gene Therapy (SR-Tiget), IRCCS San Raffaele Scientific Institute, Gene/Neural stem cell therapy for lysosomal storage diseases, 20132 Milan, Italy.
**E-mail:** meneghini.vasco@hsr.it


Published by Elsevier Inc. on behalf of The American Society of Gene and Cell Therapy.
This is an open access article under the CC BY-NC-ND license (http://creativecommons.org/licenses/by-nc-nd/4.0/).

Please cite this article in press as: Hillen et al., Targeting white matter astrocytes with a *Gfap*-disruptive Cas9 nuclease benefits a murine model of Alexander disease, Molecular Therapy (2026), https://doi.org/10.1016/j.ymthe.2026.09.019



and impair OPC maturation, contributing to progressive white matter (WM) degeneration.[23–25]

The clinical presentation of AxD is highly variable, with onset ranging from infancy to late adulthood. Magnetic resonance imaging (MRI) reflects the marked clinical heterogeneity. MRI and clinical features have been used to classify patients into infantile, juvenile, or adult[26] and more recently (integrating genetic features) into cerebral (type I), bulbospinal (type II), and intermediate (type III) groups.[27] The more severe type I disease, typically presenting during infancy or childhood, is characterized by predominant frontal WM abnormalities, whereas the later-onset type II phenotype is associated with atrophy and abnormal MRI signals in the medulla oblongata and cervical spinal cord.[27] A refined classification of type I stratifies patients into four subgroups (Ia-Id) based on longitudinal clinical follow-up data.[28] Common symptoms include motor dysfunction, seizures, macrocephaly, bulbospinal symptoms, cerebellar signs, and autonomic dysfunction.[10,29] Diagnosis is supported by MRI findings and pathogenic *GFAP* variants, while RFs remain the defining pathological hallmark.[10,26,27] Importantly, age at disease onset is one of the strongest predictors of clinical outcome. Earlier onset is associated with faster progression and poorer survival.[29] Recent genotype-informed classifications further link severity to variant pathogenicity and disease subtypes,[9,28] and meta-analyses show associations between recurrent GFAP variants, age at onset, and survival.[30,31] Notably, variants affecting arginine residues are linked with earlier onset, supporting early therapeutic intervention.

Preclinical studies have shown that antisense oligonucleotides (ASOs) targeting the 3′ UTR of *Gfap* transcripts can decrease RF aggregates and alleviate stress response and astrogliosis in a murine model of AxD.[32] The effectiveness of lowering overall GFAP levels was further highlighted by the intra-CSF administration of ASO molecules in a rat model of AxD, which improved astrocyte pathology, reduced spinal cord demyelination, and alleviated motor defects.[33] Knockdown of GFAP appears to be safe, as suggested also by studies in *Gfap* null mice.[34,35] A multiple-ascending dose clinical trial (ClinicalTrials.gov: NCT04849741) is ongoing with intrathecal bolus administration of ASOs in AxD patients.

Clustered regularly interspaced short palindromic repeat (CRISPR)-associated Cas9 nucleases offer an alternative to RNA interference by inducing permanent gene knockdown through precise DNA double-strand breaks (DSBs) at targeted genomic loci complementary to single guide RNAs (sgRNAs). Theerror-prone non-homologous end joining (NHEJ) repair pathway creates small insertions and deletions (indels), potentially resulting in frameshift mutations and premature stop codons that reduce or abolish gene expression. Clinical trials have demonstrated successful treatments through gene therapy[36] and promising outcomes for gene editing approaches.[37,38] Preclinical studies have revealed the feasibility of CRISPR-Cas9-mediated gene disruption in neural cells[39] and its potential in the treatment of neurodegenerative disorders.[40–42] However, there are currently no reports on the efficiency and efficacy of an all-in-one AAV.Cas9.sgRNA vector targeting astrocytes *in vivo* for the treatment of neurodegenerative disorders.

*Staphylococcus aureus* Cas9 (*SaCas9*) is notable for its less permissive protospacer adjacent motif (PAM), which help minimize off-target effects. Its small size makes it well-suited for incorporation in adeno-associated viral (AAV) vectors.[43,44] AAVs distribute widely in CNS tissues and are effective in delivering transgenes.[45,46] AAVs have been used in more than 66 clinical trials for neurodegenerative disorders.[47] Although AAVs rarely integrate into host genomes, recent studies indicate that DSBs induced by CRISPR-Cas9 systems can increase AAV integration rates.[48–50] These findings highlight the potential genotoxicity risks of using AAVs for CRISPR-Cas9 delivery, underscoring the need for careful evaluation of AAV integration profiles in early preclinical studies to establish a safe delivery strategy.

Following reports of successfully reverting the AxD phenotype in rodent models by targeting *Gfap* expression, we optimized the specificity and efficiency of AAV transduction in WM astrocytes to disrupt the *Gfap* gene. This was accomplished by delivering *SaCas9* and sgRNA as an all-in-one vector in a single administration in an AxD murine model. We then investigated the effects of gene editing on the primary AxD hallmarks and the rate of vector genome integrations in AxD astrocytes.

## RESULTS

### Targeting *Gfap* exon 6 with *SaCas9* nuclease downregulates protein expression in an *in vitro* AxD model

We generated an *in vitro* AxD model for efficient screening of sgRNAs knocking down *Gfap* by engineering the easily transfectable NIH3T3 cell line with a lentiviral vector (LV) expressing the murine *Gfap* coding sequence harboring the missense mutation (c.227 C>T) in exon 1. This modification results in the R76H ($GFAP^{R76H}$) mutation, which is an ortholog of the R79H GFAP mutation commonly found in patients with AxD.[51] To facilitate the detection of protein expression through fluorescence-activated cell sorting (FACS) analysis, we conjugated the $GFAP^{R76H}$ protein with an mCherry tag (LV.$GFAP^{R76H}$.mCherry; Figure S1A). Transduction of NIH3T3 cells with a low dose (MOI = 1) of LV.$GFAP^{R76H}$.mCherry, followed by FACS sorting of $mCherry^{+}$ cells, generated a cell population comprising >90% $mCherry^{+}$ cells (Figure S1B). The integrated LV copies per cell averaged 0.55 ± 0.007, as determined by digital droplet PCR (ddPCR) analyses (Figure S1B).

We designed sgRNAs targeting sequences spanning *Gfap* exons 1-6 near the *SaCas9* PAMs. Co-transfecting $GFAP^{R76H}$.mCherry-expressing cells with plasmids containing either *SaCas9* nuclease or sgRNAs showed that four sgRNAs significantly reduced mCherry expression (Figures 1A and 1B). Among them, the sgRNA SaKO8 targeting *Gfap* exon 6 induced the most pronounced knockdown of the $GFAP^{R76H}$.mCherry transgene at both the mRNA (mean ± SD: −70.5% ± 1.6%; Figure 1C) and protein (mean ± SD: −46.2% ± 12.2%; Figure 1A) levels. Sequencing of the target locus to evaluate the editing efficiency of sgRNA SaKO8 showed an

Please cite this article in press as: Hillen et al., Targeting white matter astrocytes with a *Gfap*-disruptive Cas9 nuclease benefits a murine model of Alexander disease, Molecular Therapy (2026), https://doi.org/10.1016/j.ymthe.2026.09.019



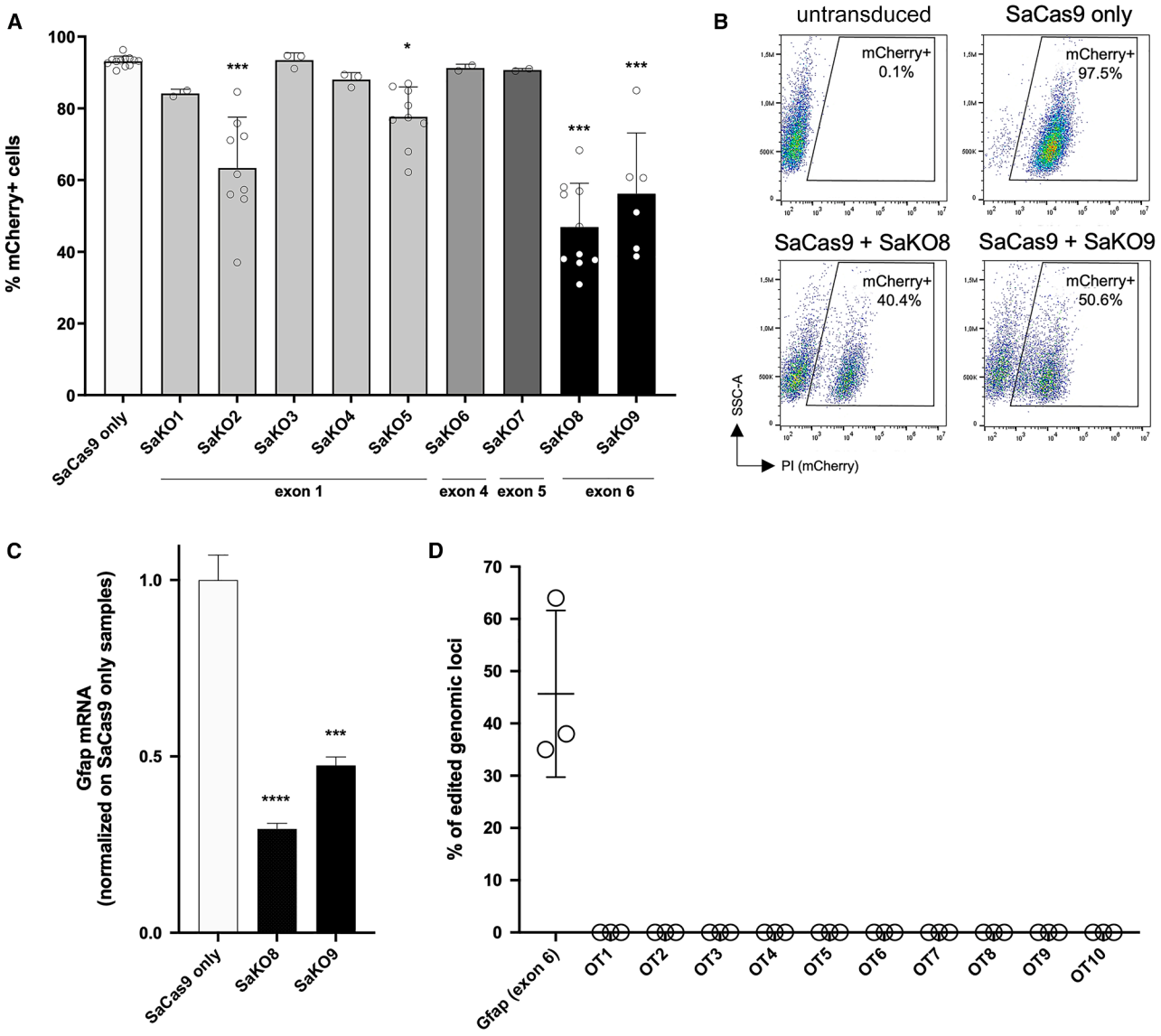



**Figure 1. Selection of sgRNAs to knock down mutant *Gfap* in engineered NIH3T3 cells**

(A) Percentage of mCherry$^{+}$ cells detected by cytofluorimetry after transfection of NIH3T3 GFAP$^{R76H}$:mCherry cells with plasmids carrying *SaCas9* nuclease and sgRNAs targeting the *Gfap*$^{R76H}$ transgene ($n$ = 2–12 replicates; each dot represents a replicate of 2–8 independent experiments). (B) Representative FACS dot plots showing NIH 3T3 GFAP$^{R76H}$:mCherry cells transfected with *SaCas9* plasmid alone (*SaCas9* only) or treated with plasmids carrying *SaCas9* nuclease and SaKO8 or SaKO9 sgRNAs. Untransduced mCherry-negative cells were used to define the gating strategy. (C) Downregulation of *Gfap*$^{R76H}$ mRNA in NIH3T3 Gfap$^{R76H}$:mCherry$^{+}$ cells transfected with plasmids carrying *SaCas9* nuclease and either SaKO8 or SaKO9. *Gapdh* was used as a housekeeping gene for normalization. Data were normalized to *Gfap* expression in *SaCas9*-only-treated samples ($n$ = 3 independent experiments). (D) Editing efficiency (% of indels) in NIH3T3 GFAP$^{R76H}$:mCherry$^{+}$ cells at the *Gfap* exon 6 locus (on-target) and the top 10 *in silico* predicted off-target loci ($n$ = 3 replicates; detailed information on off-target loci is reported in Table S5). (A–D) Data represent mean ± standard deviation. One-way ANOVA, $^{*}p < 0.05$, $^{***}p < 0.01$, $^{****}p < 0.001$ vs. *SaCas9* only-treated samples.

on-target editing rate of 45.7% ± 15.9% in the *Gfap* exon 6 (Figure 1D), as measured by the TIDE tool.[52] Additionally, no editing was observed at the top 10 *in silico* predicted off-target sites in *SaCas9*-SaKO8-treated GFAP$^{R76H}$.mCherry$^{+}$ cells (Figure 1D).

These data showed that sgRNA SaKO8 efficiently disrupted the *Gfap* gene by targeting a sequence in exon 6, which is identical in the wild-type (WT) and mutated coding sequences. On-target editing resulted in robust GFAP downregulation.

### Intracerebroventricular injection of the AAV-DJ8 vector in pups on P3 enhances astrocyte transduction in WM regions

To facilitate *in vivo* translation of our *Gfap* gene disruption strategy, we evaluated the astrocyte tropism of CNS-targeting AAV serotypes

Please cite this article in press as: Hillen et al., Targeting white matter astrocytes with a *Gfap*-disruptive Cas9 nuclease benefits a murine model of Alexander disease, Molecular Therapy (2026), https://doi.org/10.1016/j.ymthe.2026.09.019



and optimized vector administration protocols to enhance transgene expression in GFAP$^+$ astrocytes in brain regions affected by AxD pathology.

Published data show that GFAP protein and RFs progressively accumulate in the brain of *Gfap*$^{+/R76H}$ mice (AxD mice).[51] The altered rate of GFAP polymerization in AxD astrocytes results in the accumulation of monomers and dimers in the cytoplasm, leading to the formation of aberrant oligomers that bind to the cytoskeleton and intermediate filaments.[16] Western blot analysis of the soluble fraction (enriched in cytoplasmic proteins) and the insoluble fraction (enriched in cytoskeletal proteins) from brain tissue showed increased GFAP content in 1- and 3-month-old untreated (UT) AxD mice compared to age-matched WT controls (Figures S2A and S2B). Immunohistochemistry (IHC) analysis on brain slices confirmed the upregulation of GFAP expression in AxD mice. GFAP$^+$ area was moderately increased in 1-month-old animals, while the differences between transgenic and WT mice were more evident at 3 months of age (Figures S2C and S2D). Qualitative evaluations showed that the increase in the GFAP$^+$ area was primarily observed in the corpus callosum, periventricular WM, and fimbria (Figure S2C).

The GFAP accumulation in WM regions observed in various AxD models is associated with the formation of RFs.[51,53,54] A semi-quantitative evaluation of RF accumulation with hematoxylin and eosin (H&E) staining revealed eosinophilic aggregates in both gray matter and WM regions, including the olfactory bulb, subpial cortex, hippocampus, corpus callosum, and subependymal lateral ventricles. Notably, there was an age-dependent accumulation of RFs around the lateral ventricles (Figure S2E; Table S1). These findings are supported by previously published data on *Gfap*$^{+/R76H}$ mice[51] and identify specific affected brain areas that could be targeted by AAVs to enhance therapeutic outcomes.

To choose the vector ensuring optimal transduction of astrocytes in WM regions, we performed a side-by-side comparison between: (1) AAV9.PHP.eB, which has been used to deliver Cas9 nuclease to astrocytes in multiple brain regions with higher efficiency than AAV9 following neonatal intracerebroventricular (i.c.v.) injection[39] and (2) AAV-DJ8, which has a preferential tropism for glial cells.[55] We assessed the distribution and transduction efficiency of GFP-expressing AAV vectors following bilateral i.c.v. injection at postnatal day 0 (P0) in FVB WT mice ($4 \times 10^9$ genome copies (gc)/hemisphere; $n = 4$ mice/group). Immunofluorescence (IF) analysis of AAV-treated brains at 3 weeks post-injection showed a rostro-caudal distribution of AAV9.PhP.eB particles and GFP expression in several brain regions, including the olfactory bulb, cortex, hippocampus, and cerebellum in all analyzed animals (Figure 2A). Some inter-animal variability was observed, with mice showing prominent transgene expression in the caudoputamen or displaying low but detectable GFP expression in the thalamus. The administration of AAV-DJ8 resulted in transgene expression in the hippocampus and cortex, predominantly within the retrosplenial, visual, posterior parietal association, and somatosensory cortices in all analyzed animals (Figure 2A). In addition, scattered GFP-positive cells were detected in the somatosensory and orbital cortices, while lower but still detectable transduction was observed in the olfactory bulbs and cerebellum.

Importantly, a higher number of GFP$^+$GFAP$^+$ cells were detected in the hippocampus and corpus callosum of animals treated with AAV-DJ8 (Figures 2B–2D), confirming its astrocytic tropism.[55] To verify whether transduction of GFAP$^+$ cells in the periventricular regions could be further increased, we injected AAVs at P3, around the peak of post-natal astrogliogenesis.[56] Bilateral i.c.v. injections of AAV-DJ8 and AAV9.PhP.eB in WT pups at P3 ($4 \times 10^9$ gc/hemisphere; $n = 3$ mice/group) increased the percentage of GFP$^+$GFAP$^+$ cells in the hippocampus and cortex/corpus callosum by 2- to 3-fold compared to animals treated at P0 (Figures 2B–2D). In the P3 setting, AAV-DJ8 displayed the highest tropism for GFAP$^+$ cells in all analyzed areas, including the periventricular regions (Figure 2B). i.c.v. injection of AAV-DJ8 at P3 resulted overall in a reduced vector spread, while maintaining a comparable regional pattern (Figure 2A), with GFP$^+$ cells mainly detected in WM regions marked by RF accumulation in adult AxD mice (Figure S2C).

These data showed that i.c.v. injection of AAV-DJ8 in P3 pups led to high transduction rates of GFAP$^+$ astrocytes in brain regions characterized by the accumulation of GFAP protein and RF aggregates.

### Intracerebroventricular injection of an all-in-one AAV-DJ8 vector harboring *SaCas9* nuclease and SaKO8 sgRNA efficiently disrupts the *Gfap* gene in astrocytes of *Gfap*$^{+/R76H}$ mice

To restrict transgene expression specifically to astrocytes, we employed the astrocyte-specific promoter GfaABC$_1$D[57] to drive the expression of the *SaCas9* nuclease. We generated an all-in-one AAV-DJ8 vector harboring both GfaABC$_1$D-*SaCas9* and U6-SaKO8 expression cassettes (AAV.Cas9.SaKO8 vector; Figure 3A). An AAV-DJ8 vector carrying the GFP coding sequence under the GfaABC$_1$D promoter (AAV.GFP vector) served as a control (Figure 3A). We bilaterally injected the AAV.Cas9.SaKO8 or AAV.GFP vectors into the lateral ventricles of *Gfap*$^{+/R76H}$ pups at P3 ($1.4 \times 10^{10}$ gc/hemisphere; $n = 9$ mice/group) and collected tissues when the mice reached 3 months of age.

IF analyses of AAV.GFP-treated mice showed that transgene expression was predominantly observed in astrocytes, with the majority of GFP$^+$ cells expressing S100β (mean ± SD: 72.9% ± 15.8%) or GFAP (45.9% ± 10.2%) (Figure 3B; n = 4–6 mice/group). Only a small subset of GFP$^+$ cells expressed Olig2 or NeuN markers (mean ± SD: 1.3% ± 1.5% oligodendrocytes or 0.2% ± 0.4% neurons, respectively) (Figure 3B). Using ACSA-2 microbeads for cell purification from AAV-treated brains, we separated the ACSA-2$^+$ fractions, enriched in cells expressing the astrocytic markers *Aldh1l1* and *Gfap*, from ACSA-2$^-$ cell populations that included cells expressing oligodendrocytic (*Pdgfr-a*), microglial (*Tmem119*), and neuronal (*Neun*) markers (Figures S3A–S3C). In AAV.Cas9.SaKO8-treated animals, vector

Please cite this article in press as: Hillen et al., Targeting white matter astrocytes with a *Gfap*-disruptive Cas9 nuclease benefits a murine model of Alexander disease, Molecular Therapy (2026), https://doi.org/10.1016/j.ymthe.2026.09.019



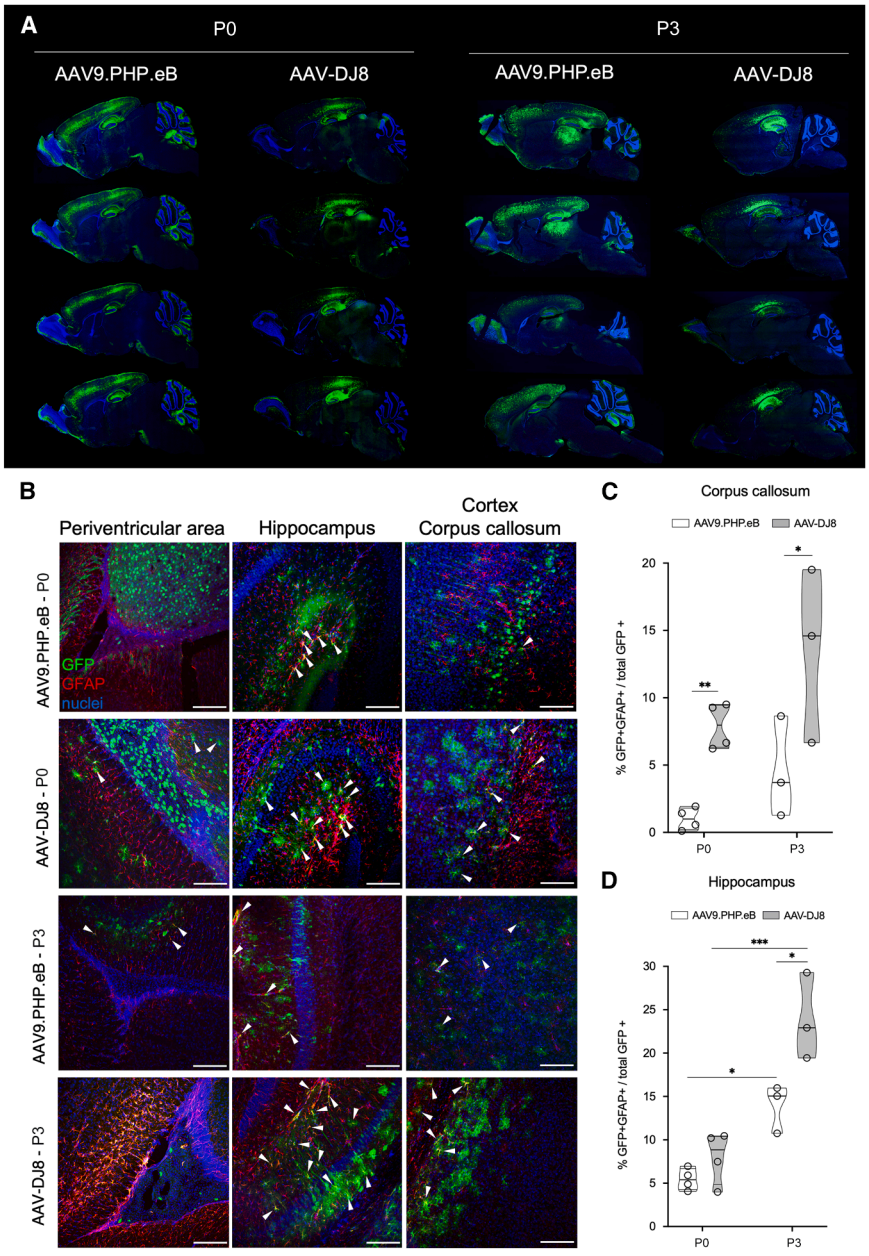



**Figure 2. Optimization of astrocyte transduction via intracerebroventricular AAV injections in neonatal mice**

(A) Representative immunofluorescence (IF) images showing GFP expression in sagittal brain slices (lateral [top] to medial [bottom] axis) of 3-week-old WT mice treated with bilateral i.c.v. injections of AAV9.PHP.eB.CBA.GFP or AAV-DJ8.CAG.GFP vectors ($4 \times 10^9$ gc/mouse) at postnatal day 0 (P0) or P3. Green, GFP; blue, Hoechst (nuclei). (B) Representative IF images showing $GFP^+$ cells in the periventricular region, hippocampus, cortex, and corpus callosum. White arrowheads indicate $GFAP^+$ astrocytes co-expressing GFP. Green, GFP; red, GFAP; blue, Hoechst. Scale bars, 200 μm. (C and D) Quantification of $GFP^+GFAP^+$ cells in the hippocampus (D) or the cortex and corpus callosum (C) of 3-week-old WT animals injected with AAV9.PHP.eB or AAV-DJ8 at P0 or P3. $n$ = 3–4 mice/group, $n$ = 1–2 hemispheres/mouse, $n$ = 2–8 sections/hemisphere, $n$ = 10–210 cells/section. Data are presented as median ± interquartile range, with each dot representing a different animal. One-way ANOVA, $^*p < 0.05$, $^{**}p < 0.01$, $^{***}p < 0.001$.

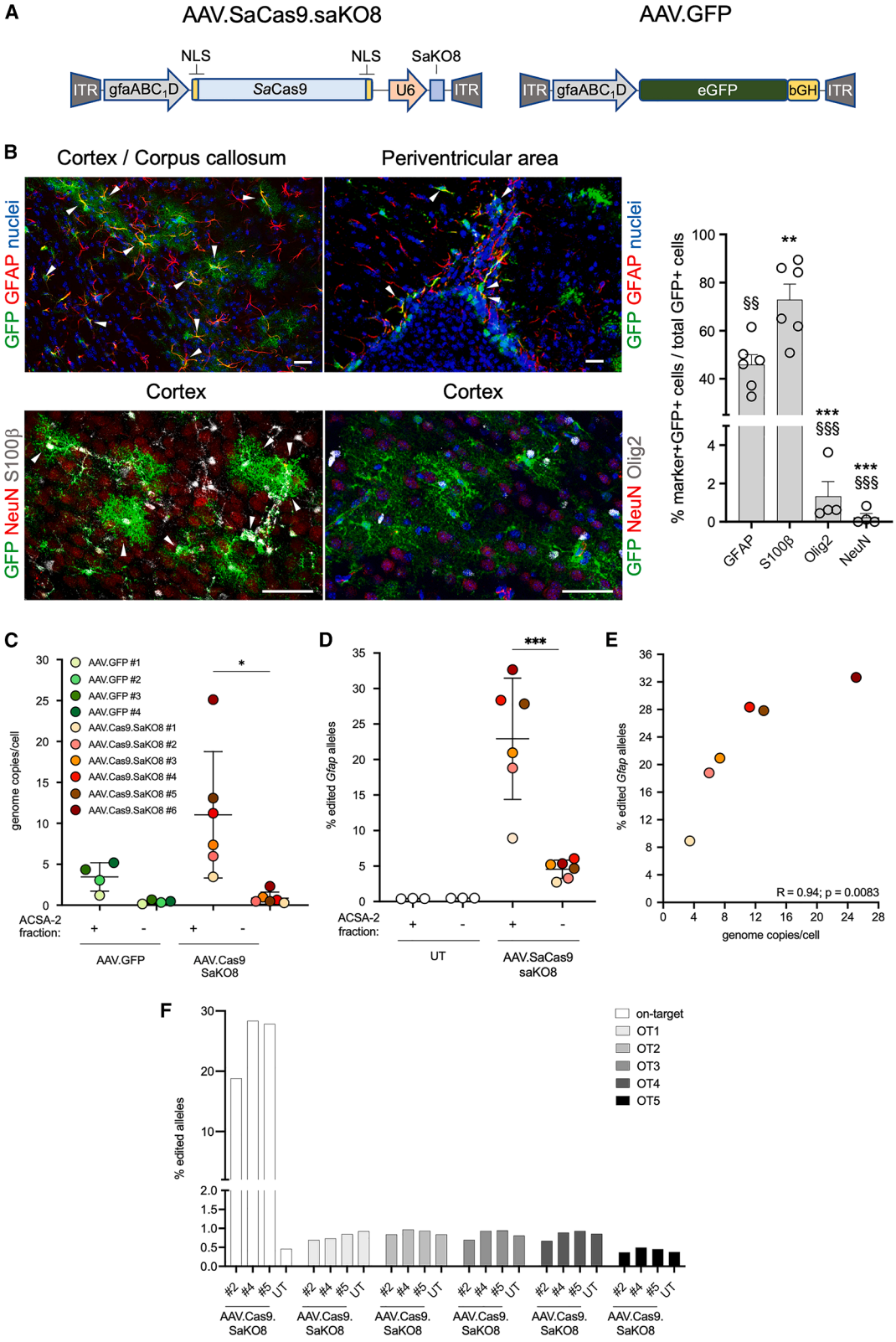
transduction efficiency was significantly higher in purified astrocytic populations (11.04 ± 7.77 gc/cell) compared to ACSA-$2^-$ counterparts (0.86 ± 0.74 gc/cell), as determined by ddPCR for AAV inverted terminal repeat (ITR) sequences ($n$ = 6 mice; Figure 3C). AAV.GFP-treated mice showed lower vector genomes per cell, yet the transduction rate of ACSA-$2^+$ cells was higher than ACSA-$2^-$ populations ($n$ = 4 mice; Figure 3C). The expression of the GFP transgene by astrocytes, along with the increased presence of vector genomes in astrocytes, supports our findings of a preferential astrocytic tropism of AAV-DJ8 vectors.

To determine whether AAV.Cas9.SaKO8 induced significant editing in astrocytes, we analyzed the percentage of small indels at the on-target locus by performing deep sequencing of *Gfap* alleles. CRISPResso2 analysis[58] revealed editing rates of up to 32.7% in *Gfap* exon 6 (mean ± SD = 22.9% ± 8.54%; $n$ = 6; Figure 3D). The majority of these indels consisted of 1-base pair (bp) deletions or 1-bp insertions at the *Sa*Cas9 cutting site (Figure S3D), leading to frameshift mutations that likely resulted in premature stop codons in exon 6 of *Gfap*. Long-read sequencing of the *Gfap* locus corroborated the CRISPResso2 analysis, revealing a comparable frequency of insertion and deletion events (Figure S3E), with the majority of edited alleles carrying 1-bp insertions or deletions (Figure S3F). Notably, we observed a significant positive correlation between the number of AAV genomes per cell and the editing efficiency in ACSA-$2^+$ fractions isolated from AAV.Cas9.SaKO8-treated brains (Figure 3E).

GUIDE-seq analysis performed in a murine cell line identified potential off-target sites, the majority of which were located within intergenic or intronic regions and contained >5 mismatches relative to the gRNA sequence (Table S2). To evaluate SaKO8 off-target activity in AAV.Cas9.SaKO8-treated mice, we deep-sequenced the top five off-target sites and detected negligible, nearly undetectable editing in transduced astrocytes (Figure 3F). Consistent with these findings,

Please cite this article in press as: Hillen et al., Targeting white matter astrocytes with a *Gfap*-disruptive Cas9 nuclease benefits a murine model of Alexander disease, Molecular Therapy (2026), https://doi.org/10.1016/j.ymthe.2026.09.019






*(legend on next page)*

Please cite this article in press as: Hillen et al., Targeting white matter astrocytes with a *Gfap*-disruptive Cas9 nuclease benefits a murine model of Alexander disease, Molecular Therapy (2026), https://doi.org/10.1016/j.ymthe.2026.09.019



long-read sequencing detected no evidence of large on-target deletions (Figure S3F) or genomic translocations involving the *Gfap* locus.

Combining the GfaABC$_1$D promoter and AAV-DJ8 serotype resulted in preferential transgene expression in AxD astrocytes, leading to robust editing at the targeted *Gfap* locus.

### Editing of the *Gfap* gene reduces RFs in WM regions of *Gfap*$^{+/R76H}$ mice

To evaluate the downstream effects of gene editing at the *Gfap* locus, we evaluated the extent of *Gfap* downregulation at both the mRNA and protein levels. In the ACSA-2$^+$ fractions, we found a significant decrease in *Gfap* mRNA levels in mice treated with AAV.Cas9.SaKO8 compared to animals treated with AAV.GFP (Figure S4A; $n$ = 6–7 mice/group). At the protein level, western blot analysis on the soluble and insoluble brain protein fractions revealed a significant reduction in GFAP content in AAV.Cas9.SaKO8-treated mice when compared to untreated (UT) and AAV.GFP-treated AxD animals (Figures 4A and 4B; $n$ = 6–9 mice/group). Of note, gene editing normalized GFAP content to near WT levels in five out of nine animals (Figure 4A). The downregulation of GFAP protein following Cas9-targeting of the *Gfap* gene was further confirmed by IHC analysis (Figures 4C and 4D). A significant reduction in GFAP$^+$ areas in the periventricular WM and the corpus callosum was detected in AAV.Cas9.SaKO8-treated animals compared to controls (Figure 4D; $n$ = 3–5 mice/group). These findings suggest potential effects on the RF accumulation in these WM regions. Indeed, when we quantified the number of cells associated with RFs, we found that AAV.Cas9.SaKO8 significantly reduced the accumulation of eosinophilic protein aggregates (Figures 4E and 4F; Figure S4B; $n$ = 5–7 mice/group). A similar trend was observed when quantifying the total number of RFs in these WM areas (Figures S4C and S4D).

Since GFAP accumulation and RF formation have been linked to enhanced astrogliosis in other AxD models,[33,51,53] we investigated the effects of Cas9 treatment on the expression of inflammatory (*Timp1* and *Ccl2*) and neurodegenerative (*Lcn2*) markers that are upregulated in AxD.[33,53,54,59] We observed a trend of reduced expression of these astrogliosis-associated factors in the ACSA-2$^+$ astrocytes of animals treated with AAV.Cas9.SaKO8 compared to controls (Figure S4E; $n$ = 5–7 mice/group).

Our data indicate that Cas9 nuclease-mediated knockdown of GFAP leads to reduced AxD pathology in WM regions, including RF accumulation and reactive astrogliosis.

### AAV vector integrates into the genome of transduced astrocytes, preferentially in the *Gfap* on-target locus

Because AAV vectors have the propensity to integrate into the genome of transduced cells,[49,60] we performed sonication and ligation mediated (SLiM)-PCR to uncover potential integration events in an unbiased genome-wide manner. SLiM-PCR was performed with primers targeting the AAV ITRs on the genomic DNA of ACSA-2$^+$ astrocytes isolated from AAV.GFP- or AAV.Cas9.SaKO8-treated brains ($n$ = 3–5 animals/group). Integration site (IS) analysis performed with the RAAVioli pipeline[61] identified a limited number of unique AAV ISs in treated animals (Figure 5A; Figure S5A). These events occurred more frequently in AAV.SaCas9.SaKO8-transduced astrocytes (Figure 5A; Figure S5A) and positively correlated with the number of vector genomes per cell (Figure 5B; Figure S5B) and editing rates detected in ACSA-2$^+$ cells (Figure 5C; Figure S5C). Of note, a high abundance of AAV.Cas9.SaKO8 ISs were observed within *Gfap* exon 6 (Figure 5D), with ITRs detected near the Cas9 nuclease cleavage site (Figure S5D). Long-range SLiM-PCR confirmed the occurrence of AAV integrations both upstream and downstream of the nuclease cleavage site within the *Gfap* exon 6 (Figure S5E).

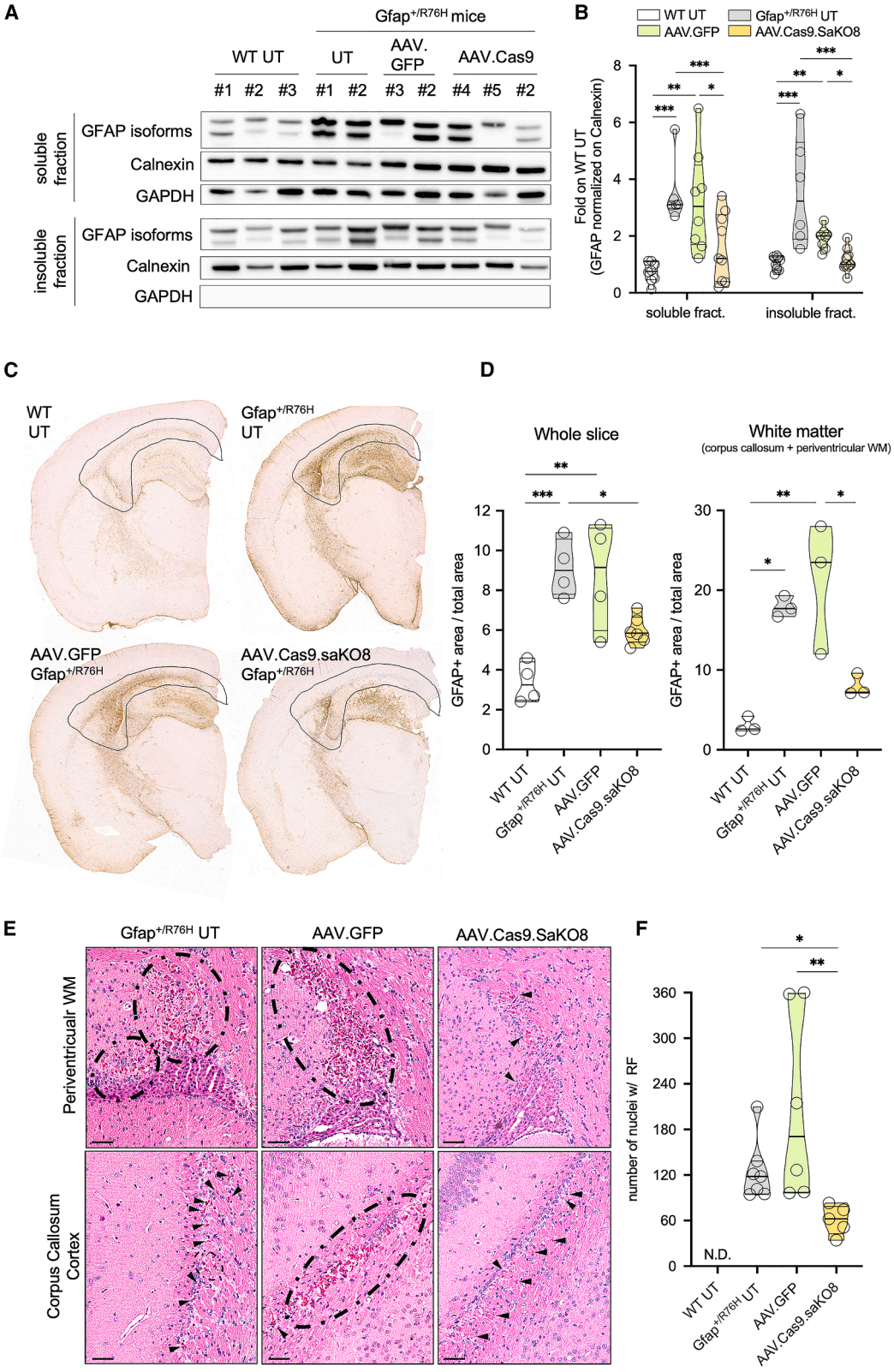
Apart from the integrations observed in *Gfap* exon 6, AAV vectors almost exclusively integrated in introns or intergenic regions of astrocyte genomes in both AAV.GFP- and AAV.Cas9.SaKO8-treated mice (Figure 5E). Notably, no ITR-integrating loci were shared between astrocytes of different AAV-treated animals, excluding the SaKO8 on-target locus. Because the ITR primers were designed in reverse orientation, the detection of integrated transgene cassettes (GFP or Cas9 nuclease) suggests the occurrence of rearrangements of the viral genome or insertion of AAV concatemers (Figure 5F). Long-range SLiM-PCR showed that the transgene cassette, or fragments thereof (including the GfaABC1D promoter, *SaCas9*, and bGH polyA sequences), integrates within the *SaCas9* cleavage site, with no evidence of integration of plasmid sequences used for AAV production (Figure S5F). Integrated AAV sequences predominantly consisted of a single AAV genome, or portions thereof, although concatemeric integrations were also detected within the *Gfap* exon 6 (Figure S5G).

**Figure 3. AAV transduction and gene editing efficiencies in astrocytes of *Gfap*$^{+/R76H}$ mice**

(A) Schematic overview of the AAV.Cas9.SaKO8 and AAV.GFP vectors, which were injected bilaterally ($1.4 \times 10^{10}$ gc/hemisphere) into the lateral ventricles of *Gfap*$^{+/R76H}$ pups at P3. ITR, AAV inverted terminal repeat; gfaABC$_1$D, minimal Gfap promoter; NLS, SV40 nuclear localization sequence; U6, U6 promoter; bGH, bovine growth hormone polyadenylation signal. (B) Representative confocal images showing GFP$^+$ cells in the periventricular area, corpus callosum, and cortex of AAV.GFP-treated mice 3 months after treatment. White arrowheads indicate the co-localization of GFP with cell-specific markers for astrocytes (S100β, GFAP), oligodendrocytes (Olig2), and neurons (NeuN). Scale bars, 100 μm. The bar graph provides a quantitative analysis of GFP$^+$ cells co-expressing cell-specific markers ($n$ = 4–6 animals/group; $n$ = 3 sections/animal, 4–8 images/section, 56–523 GFP$^+$ cells/section). One-way ANOVA, $^{**}p < 0.01$, $^{***}p < 0.001$ vs. GFP$^+$GFAP$^+$ cells, §§$p < 0.01$, §§§$p < 0.001$ vs. GFP$^+$S100β$^+$ cells. (C) Number of AAV genome copies per cell (gc/cell) in ACSA-2$^+$ and ACSA-2$^-$ fractions of AAV.GFP- and AAV.Cas9.SaKO8-treated animals ($n$ = 4–6 mice). Kruskal-Wallis, $^{*}p < 0.05$. (D) Percentage of edited *Gfap* alleles (% of indels) in the ACSA-2$^+$ and ACSA-2$^-$ fractions of AAV.Cas9.SaKO8-treated ($n$ = 6 mice) and untreated (UT; $n$ = 3) AxD mice, as determined by CRISPResso2 analysis. Unpaired Student's $t$ test, $^{***}p < 0.001$. (E) Correlation between AAV transduction (shown in C) and gene editing (shown in D) efficiencies in ACSA-2$^+$ fractions of AAV.SaCas9-SaKO8-treated animals ($n$ = 6 mice). Spearman correlation. (F) Deep-sequencing analysis of the top 5 GUIDE-seq-identified off-target (OT) loci in ACSA-2$^+$ astrocytes purified from AAV.SaCas9-SaKO8 #2, #4, and #5 mice and an untreated (UT) *Gfap*$^{+/R76H}$ animal. Detailed information on OT1-5 is reported in Table S2. (B–D) Data are presented as mean ± standard deviation. Each dot represents a different animal with the same color coding in (C), (D), and (E).

Please cite this article in press as: Hillen et al., Targeting white matter astrocytes with a *Gfap*-disruptive Cas9 nuclease benefits a murine model of Alexander disease, Molecular Therapy (2026), https://doi.org/10.1016/j.ymthe.2026.09.019






*(legend on next page)*

Among 132 unique ISs detected in AAV-treated animals, integrated ITRs were observed in two genes associated with potential oncogenesis, each reported in a different AAV.SaCas9.SaKO8-treated mouse. AAV genomes were detected in *Egfr* intron 20 (AAV.SaCas9.SaKO8 #3 mouse) and *Brca1* intron 2 (AAV.SaCas9.SaKO8 #2 mouse) (Figure S5H). Of note, the abundance of AAV genome counts detected at these unique ISs was relatively low (*Egfr*: 11 out of 147 genome counts; *Brca1*: 4 out of 64 genome counts), and it is unlikely to be correlated with the expansion of tumorigenic cell clones. Indeed, histopathological analyses in the brains of AAV.Cas9.SaKO8-treated mice revealed the absence of tumors 3 months post-treatment.

## DISCUSSION

Given the central role of astrocytes in driving AxD pathology, we have optimized strategies to enhance AAV-mediated transgene expression preferentially within this glial cell population. Data obtained from WT mice indicate that the AAV-DJ8 vector preferentially targets murine GFAP$^+$ astrocytes, and this targeting can be further increased by administering the vector into the CSF at the peak of postnatal astrogenesis. Notably, the strong astrocytic tropism of the AAV-DJ8 vector has been confirmed in human brain organotypic slices derived from resected neurosurgical specimens, with a trend toward higher transduction efficiency in samples obtained from pediatric donors.[62] These findings from short-term experiments in WT animals were successfully translated to *Gfap*$^{+/R76H}$ mice, achieving astrocyte-preferential GFP expression by combining AAV tropism, i.c.v. injection at P3, and an engineered minimal *GFAP* promoter.[57] This *in vivo* setting resulted in robust transduction of S100β$^+$ and GFAP$^+$ astrocytes in the corpus callosum and periventricular area, with minimal detection of transgene expression in oligodendrocytes and neurons. These observations align with previously published data showing GFP expression in astrocytes of the substantia nigra following i.c.v. injection of AAV.GfapABC$_1$D.GFP at P0,[55] and increased vector transduction of glial cells when AAVs were administered at postnatal ages.[63] The peak of human astrogenesis occurs during late gestation and, to a lesser extent, continues into the postnatal period, with ventricular and subventricular zones retaining astrocytic proliferation throughout life.[64] Clinical trials with intra-CSF AAV administration have enrolled pediatric patients from 6 months of age,[65] which falls within the wide age range of disease onset in the AxD patient population.[28] Since intra-CSF injection, particularly i.c.v. administration, results in efficient AAV transduction of the ventricles in non-human primates,[66,67] we speculate that administering AAV vectors during early postnatal development may likewise favor astrocyte transduction in humans. Future studies in non-human primates will be essential to define the optimal route of administration (intra-CSF vs. intraparenchymal), vector tropism and dosing, and age at treatment required to achieve therapeutically meaningful astrocyte transduction in WM regions affected by AxD pathology in humans.

A previous report identified sgRNAs recognized by *Streptococcus pyogenes* Cas9 (*SpCas9*) nuclease that downregulated GFAP expression in CNS tissues of transgenic mice constitutively expressing the editing enzyme.[39] However, the clinical translation of NHEJ-based approaches exploiting *SpCas9* requires co-injection of a dual AAV system, potentially reducing the transduction and editing rates in target cells while increasing vector doses.[68] Here, a single administration of an all-in-one AAV.Cas9.SaKO8 vector resulted in robust editing of the *Gfap* gene in astrocytes. The high editing efficiency of SaKO8 in engineered cell lines was mirrored by the gene disruption observed in ACSA-2$^+$ astrocytes isolated from AxD brains. We found a direct correlation between transduction and editing efficiency in the mouse brain, achieving up to 32% of alleles modified at the on-target locus within *Gfap* exon 6. These findings underscore the need for high transduction efficiency and strong Cas9 nuclease expression in CNS target cells to reach relevant editing rates. Although this viral platform achieved high on-target efficiency, stronger constitutive promoters combined with astrocyte-specific miRNA de-targeting strategies may further increase *SaCas9* nuclease expression in poorly transduced astrocytes.[69] Alternatively, intra-CSF administration could be combined with intraparenchymal injections to enhance AAV biodistribution in WM regions.[70]

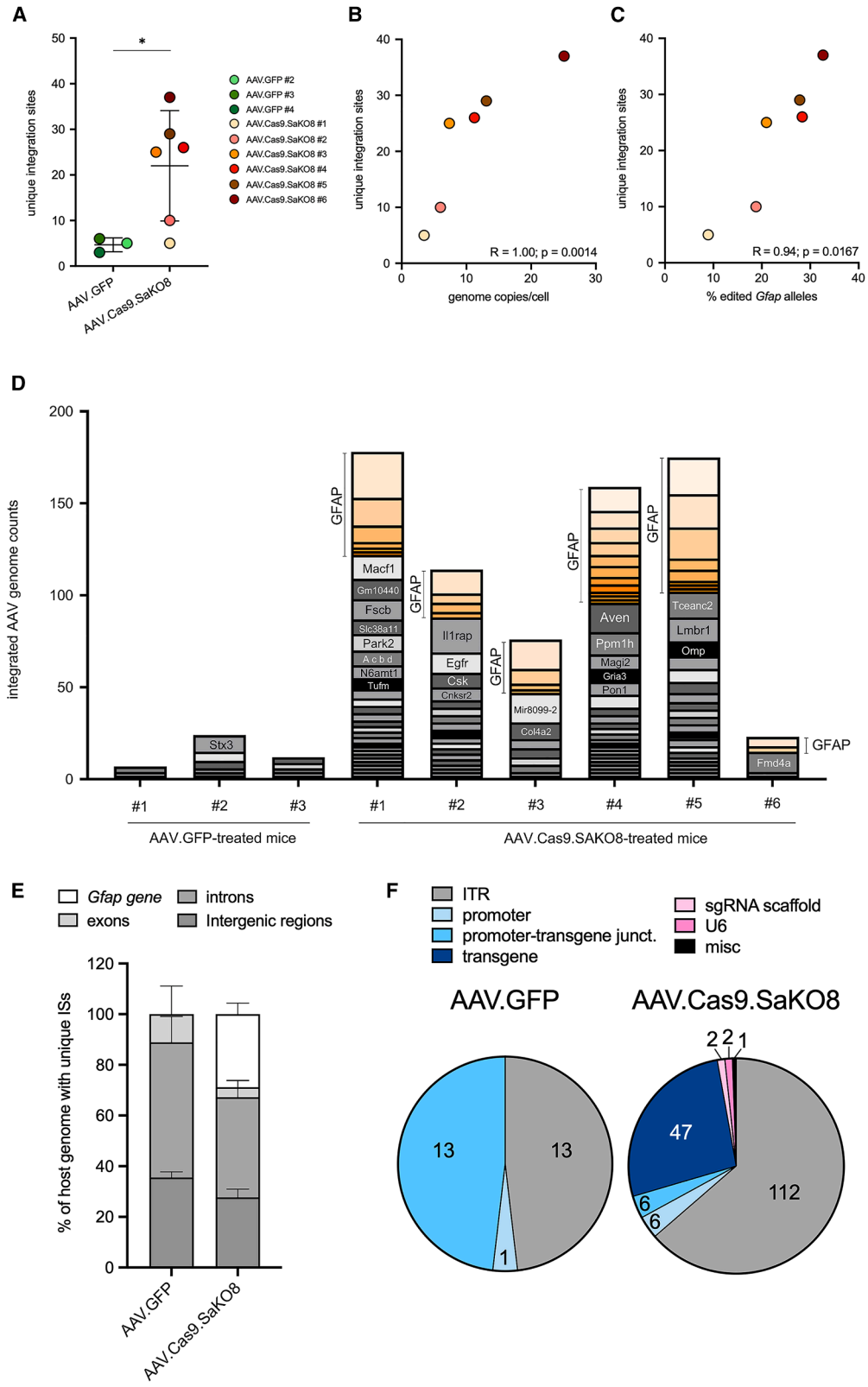
GFAP overproduction plays a crucial role in both the induction and maintenance of AxD pathology.[12,71] Deep-sequencing analyses on ACSA2$^+$ astrocytes showed that Cas9 nuclease primarily induces 1 bp insertions and deletions at the on-target locus within the *Gfap* coding sequence. These events result in frameshift mutations that can produce *de novo* stop codons. Our data from both *in vitro* and *in vivo* studies indicate decreased *Gfap* mRNA levels following *SaCas9* treatment. *In vivo* experiments with AAV.Cas9.SaKO8 demonstrated a reduction of both soluble and insoluble GFAP proteins in brain protein extracts. These data support the hypothesis that the

**Figure 4. Effect of AAV.Cas9.SaKO8 treatment on AxD phenotypes**

(A and B) Representative western blots (A; $n$ = 2–3 animals/group; #1, #2, #3) and quantification (B; $n$ = 6–9 mice/group) of the amount of GFAP isoforms in soluble (cytoplasmic) and insoluble (cytoskeletal) protein fractions purified from brains of untreated (UT) WT and *Gfap*$^{+/R76H}$ mice and AAV-treated *Gfap*$^{+/R76H}$ animals at 3 months of age. GAPDH was used as a cytoplasmic marker, detectable only in soluble fractions. Calnexin served as a housekeeping protein for quantifying total GFAP signals (both isoforms). One-way ANOVA, $^*p < 0.05$, $^{**}p < 0.01$, $^{***}p < 0.001$. (C) Representative images of immunohistochemistry (IHC) analysis for GFAP expression in coronal brain slices of UT and AAV-treated animals at 3 months of age. (D) The GFAP signal from IHC analysis was quantified by measuring the GFAP$^+$ pixel area and normalizing it to the total pixel area. The quantification was performed on whole brain slices (left graph) and selectively in white matter (WM) regions (corpus callosum and periventricular WM; right graph), as indicated by the black lines in (C). $n$ = 4–6 mice/group, $n$ = 3–6 slices/animal. One-way ANOVA, $^*p < 0.05$, $^{**}p < 0.01$, $^{***}p < 0.001$. (E) Representative images showing Rosenthal fibers (RFs) in the corpus callosum and periventricular area of UT or AAV-treated AxD animals at 3 months of age. RFs appear as amorphous eosinophilic aggregates in H&E staining, with arrows indicating a single RF and circles indicating clusters. Scale bars, 200 μm. (F) Quantification of the total number of nuclei detected in close proximity to RFs in the periventricular WM and the corpus callosum. $n$ = 5–7 mice/group, $n$ = 3–5 slices/animal. Kruskal-Wallis, $^*p < 0.05$, $^{**}p < 0.01$. N.D., not detected. (B–F) Data represent median ± interquartile range. Each dot represents a different animal.

Please cite this article in press as: Hillen et al., Targeting white matter astrocytes with a *Gfap*-disruptive Cas9 nuclease benefits a murine model of Alexander disease, Molecular Therapy (2026), https://doi.org/10.1016/j.ymthe.2026.09.019






*(legend on next page)*

formation of *de novo* stop codons in *Gfap* exon 6 induces GFAP downregulation through nonsense-mediated mRNA decay and/or proteasomal degradation of misfolded proteins.[34,35,72–74] This argues against generating a stable truncated GFAP protein that could worsen GFAP aggregation.

Our findings confirmed previous observations in ASO-treated rodents,[32,33] highlighting the central role of GFAP in AxD pathology and the efficacy of therapies targeting the expression of both the mutated and WT *Gfap* allele. Both GFAP mutations and overexpression of the WT protein lead to the formation of RFs and the activation of stress response in astrocytes,[75,76] suggesting a threshold of GFAP toxicity.[12] Intra-CSF administration of ASOs targeting the 3′-UTR of both WT and mutated *Gfap* mRNA effectively mitigates pathological signs by substantially reducing total GFAP expression to near-undetectable levels.[32,33] Similarly, gene editing aimed at permanently knocking out the GFAP protein in affected astrocytes reduces the formation of cytoplasmic protein aggregates and decreases the expression of inflammatory and neurodegenerative markers in these cells. Although the implications of significant *GFAP* downregulation in humans remain unclear, data collected in *Gfap* null mice indicate that the absence of GFAP protein does not have detrimental effects under physiological conditions. *Gfap* null mice show increased susceptibility to CNS injury, such as heightened vulnerability of the vasculature to trauma and ischemia, but these animals retain normal lifespan, brain development and architecture, and blood-brain-barrier integrity.[34,35,72–74] This suggests that other intermediate filaments, such as vimentin, may activate compensatory mechanisms.[34]

I.c.v. injection of AAV.Cas9.SaKO8 vector benefits $Gfap^{+/R76H}$ mice but results in only a partial rescue of pathological hallmarks. The levels of astrogliosis markers remain elevated relative to those in age-matched WT animals. The rescue appears to correlate with the number of successfully transduced astrocytes, likely reflecting the more limited vector spread compared with ASO distribution in mice.[32] A significant portion of AxD pathology arises from astrocytic dysfunction, which disrupts the brain microenvironment and ultimately contributes to neurodegeneration and demyelination. AxD astrocytes release neurotoxic molecules that affect neuronal survival, as well as pro-inflammatory cytokines, such as CHI3L1, which impair the proliferation and maturation of oligodendrocyte progenitors.[25,54,77] Some therapeutic effects may, therefore, occur in a non-cell-autonomous manner, whereby alleviating AxD pathology in a subset of astrocytes could confer broader benefits to the brain microenvironment. However, it remains unclear whether the editing rates achieved here are sufficient to mitigate the non-cell-autonomous phenotypes, particularly because the $Gfap^{+/R76H}$ model has milder phenotypes[51] and does not display microgliosis, neurodegeneration, or demyelinating symptoms. Future dose-escalation studies on $Gfap^{+/R237H}$ rats, which exhibit microglial reactivity, WM abnormalities, and motor symptoms,[33] will be crucial to determine the safest AAV.Cas9.SaKO8 dose capable of alleviating the full spectrum of AxD-related pathology and functional deficits.

The favorable safety profile of our AAV platform was underscored by low levels of vector integration in GFP-treated animals. Our analyses in AAV.Cas9.SaKO8-transduced astrocytes confirmed previous reports in other CNS cells showing enhanced ITR integration at DSBs.[49,50] No locus other than the sgRNA target site was recurrent across multiple animals, suggesting that AAV integrations outside the *Gfap* locus were primarily stochastic events that correlated with vector genome copy number and editing rates, as reported in previous studies.[49,50] In this short-term study, the low number and abundance of unique ISs per animal argue against clonal expansion of tumorigenic cells in AAV-treated brains, as confirmed by histopathological analyses. Additionally, AAV-mediated delivery of *SaCas9* nuclease in astrocytes resulted in negligible off-target activity at the top five GUIDE-seq-identified loci. Long-read sequencing of the *Gfap* editing locus reported the absence of genomic translocation events and on-target large deletions. Although these findings provide encouraging preliminary evidence of safety, long-term *in vivo* studies will be required to fully assess the risks associated with AAV-mediated Cas9 delivery to astroglial populations, particularly given their heightened proliferative capacity during postnatal brain development. Future *in vitro* studies with human AxD models should also establish the genotoxicity in the human genome before clinical translation of this approach. These considerations are especially relevant for therapeutic applications in pediatric patients, who are most severely affected by the disease. Notably, alternative DSB-independent genome editing approaches may be considered to reduce the frequency of AAV genome integration within the host genome.

Our study underscores the promising potential of AAV-mediated delivery of the CRISPR-Cas9 system in astrocytes. Beyond the *SaCas9* nuclease, emerging compact gene editing enzymes hold

**Figure 5. Integration of AAV vector sequences in the genome of astrocytes**

(A) Number of unique AAV ITR integration sites in ACSA-$2^+$ astrocytes purified from AAV.GFP- or AAV.SaCas9.SaKO8-treated mice. Each colored dot represents a different animal. Data represent mean ± standard deviation. Unpaired Student's *t* test, $^*p < 0.05$. (B and C) Correlations between the number of unique ITR integration sites (shown in A) and (B) AAV transduction efficiency (shown in Figure 3C) or (C) gene editing efficiency (% of indels) at *Gfap* exon 6 (shown in Figure 3D) in ACSA-$2^+$ cells purified from AAV.SaCas9.SaKO8-treated animals. Spearman correlation. (D) Bar graph reporting the counts of integrated AAV genomes for each genomic locus detected in ACSA-$2^+$ cells purified from AAV.GFP- or AAV.Cas9.SaKO8-treated animals. The genomic locus name is indicated if an abundance of $n > 5$ genome counts was detected. The only recurring genomic locus between animals was the *Gfap* gene (orange scale). (E) Bar graph reporting the percentage of AAV ITRs integrated within the on-target locus (*Gfap* gene), exons and introns of other genes, and intergenic regions in ACSA-$2^+$ cells of AAV.GFP- ($n = 3$) and AAV.Cas9.SaKO8-treated ($n = 6$) animals. Data represent mean ± standard deviation. (F) Pie charts showing the percentage of AAV fragments detected in the genomic DNA of ACSA-$2^+$ cells isolated from AAV.GFP- ($n = 3$ mice) and AAV.Cas9.SaKO8-treated ($n = 6$ mice) animals.

Please cite this article in press as: Hillen et al., Targeting white matter astrocytes with a *Gfap*-disruptive Cas9 nuclease benefits a murine model of Alexander disease, Molecular Therapy (2026), https://doi.org/10.1016/j.ymthe.2026.09.019



promise for efficient CNS delivery via all-in-one AAVs, thereby expanding therapeutic options for achieving GFAP knockdown in AxD astrocytes.[68,78–83] We observed significant and persistent beneficial effects from *Gfap* editing performed in *Gfap*$^{+/R76H}$ neonatal mice, reinforcing that early intervention is crucial for therapeutic efficacy. This aligns with previous preclinical studies with ASOs in rodent AxD models,[33] as well as with clinical outcomes of gene therapy clinical trials in patients affected by other leukodystrophies.[84] Notably, a negative correlation between plasma biomarkers, such as neurofilament light chain and GFAP, and age at collection has been reported in both early- and late-onset patients with AxD.[14] Although longitudinal studies are still needed, these findings suggest that the identification of peripheral biomarkers may support earlier AxD diagnosis, thereby enabling timely therapeutic intervention in patients.

The proposed gene editing approach benefits from the advantage of single-dose treatments avoiding lifelong ASO administration, especially when considering that the AxD patient population is primarily pediatric. The clinical development of gene editing strategies disrupting the *GFAP* gene may require the optimization of nanoparticle (NP) formulations with astrocyte tropism to ensure a transient expression of the editing enzyme in target cells and avoid the risk of vector genome integration. Intraparenchymal injection of selected NPs could be envisioned as a treatment to target specific brain areas, since the new classification system of patients with AxD shows a regionalization of the pathology.[27,85] Notably, gene editing could be combined with ASOs to potentiate their efficacy and durability by reducing drug doses and improving the long-term benefit-risk balance.

## MATERIALS AND METHODS

### Design and testing of sgRNAs targeting the *Gfap* coding sequence in NIH3T3 cells

We designed sgRNAs recognized by *SaCas9* targeting exons 1–6 of the WT and mutated *Gfap* sequences. The sequences of sgRNAs are reported in Table S4.

To evaluate the on-target editing on mutated *Gfap* sequence, we transfected GFAP$^{R76H}$-mCherry NIH3T3 cells with a plasmid carrying the *SaCas9* nuclease (pSaCas9_GFP; Addgene #64709) and a plasmid carrying each sgRNA cloned into BsmBI sites (BPK2660; Addgene #70709).

Cells were expanded for 48 h, enzymatically detached, and 200,000 cells were transfected with *SaCas9* and sgRNA plasmids (0.6 pmol and 0.8 pmol, respectively) through SG Cell Line 4D-Nucleofector X Kit (Lonza) and Amaxa 4D Nucleofector X, program EN-158. After transfection, cells were plated in culture medium + Y-27632 (10μM; StemCell Technologies) for 48 h and collected at confluency. A Cytoflex S cytometer (Beckman Coulter) was used to analyze the percentage of mCherry$^{+}$ cells in transfected samples. Cells treated with the *SaCas9* plasmid alone served as a negative control. Untransduced NIH3T3 mCherry-negative cells were used as controls to define the gating strategy. Data were analyzed with FlowJo software (v.10.8.1).

### AAV vector design, production, and titer

AAV9.PHP.eB.CBA.GFP vector (AAV9.PhP.eB) was produced in 293T cells by polyethylenimine co-transfection of three different plasmids: the gene transfer vector, PhP.eB packaging plasmid, and pHelper (Agilent). Cells were lysed in hypertonic buffer containing 100 U/mL Salt Active Nuclease (SAN, Arcticzymes) for 1 h at 37°C, whereas the viral particles present in the supernatant were concentrated with 8% PEG8000 (Sigma-Aldrich) by precipitation. The viral phase was isolated by iodixanol step gradient (15%, 25%, 40%, 60% Optiprep, Sigma-Aldrich) in the 40% fraction and concentrated in PBS (phosphate-buffered saline) with 100K cut-off concentrator (Amicon Ultra15, MERCK-Millipore). Virus titers were determined with AAVpro Titration Kit Ver2 (TaKaRa). AAV-DJ8.CAG.eGFP (AAV-DJ8) was purchased from Vector Biolabs (#7118; titer $1 \times 10^{13}$ gc/mL). AAV-DJ8.GFAP(0.7).eGFP (AAV.GFP) was purchased from Vector Biolabs (#VB1149; titer $8.1 \times 10^{12}$ gc/mL). AAV-DJ8.GFAP(0.7).SaCas9.U6.SaKO8 (AAV.Cas9.SaKO8) was purchased from Vector Biolabs (titer $6.9 \times 10^{12}$ gc/mL). Sequence information is available upon request.

### Animals

A knock-in AxD mouse model containing an R76H missense mutation (c.227 C>T) in heterozygosis within exon 1 of the *Gfap* gene[51] was purchased from The Jackson Laboratory (FVB.129S7(Cg)-*Gfap*$^{tm3Mes}$/Mmjax, MMRRC stock #37136). *Gfap*$^{tm3Mes/+}$ animals are henceforth referred to as *Gfap*$^{+/R76H}$ or AxD animals. FVB.129S7(Cg) was purchased from Charles River and served as WT controls. Animals were housed in the San Raffaele Scientific Institute animal facility in Milan, Italy. All experiments and procedures described in this study involving mice were performed according to protocols approved by the internal Institutional Animal Care and Use Committee and reported to the Italian Ministry of Health, as required by Italian law (IACUC # 1221).

### Intracerebroventricular injection of AAV vectors and tissue collection

Bilateral i.c.v. injections of AAV vectors were performed in *Gfap*$^{+/R76H}$ and WT pups at doses and time points reported in the manuscript. Injection site coordinates at P0 and P3 were based on an established protocol for P0 pups,[86] using the lambda suture and eyes as landmarks to identify a location targeting the lateral ventricle (2/5$^{th}$ of the distance between lambda and the eye). The dorsal-ventral coordinate ranged from −1.6 to −1.8 mm.

WT animals treated with AAV9.PHP.eB.CBA.GFP and AAV-DJ8.CAG.eGFP ($4 \times 10^{9}$ gc/hemisphere) at P0 and P3 were euthanized three weeks post-injection, and brains were fixed in 4% paraformaldehyde (PFA) to evaluate GFP expression by IF analyses.

*Gfap*$^{+/R76H}$ animals treated with AAV-DJ8.GFAP(0.7).eGFP and AAV-DJ8.GFAP(0.7).SaCas9.U6.SaKO8 ($1.4 \times 10^{10}$ gc/hemisphere) at P3 were euthanized three months post-injection. Age-matched untreated WT and *Gfap*$^{+/R76H}$ served as controls. Brains were collected, dissected into hemispheres, and each hemisphere was

randomly assigned: for fixation in 4% PFA for IF analyses, fixation in formalin for immunohistochemistry analyses, collection of snap-frozen tissues (telencephalic areas) for biochemical analysis, or isolation of $ACSA^+$ and $ACSA^-$ cells from the telencephalon.

Alternatively, hemispheres were cut coronally into three pieces, dissecting the olfactory bulb and the cerebellum away from the remainder of the brain. These three sections were snap-frozen, or the middle section was dissociated to a single-cell suspension with the Adult Brain Dissociation kit (Miltenyi).

#### Deep sequencing and CRISPResso2 analysis

A total of 50 ng of genomic DNA isolated from $ACSA\text{-}2^+$ cells was used to amplify fragments surrounding the on-target locus and off-target loci (Table S2) by using GoTaq G2 DNA Polymerase (Promega) and primers for the genomic locus conjugated to Illumina adapter sequences (Table S3). PCR was performed with the following conditions: 95°C for 3 min; 30 cycles: 95°C for 45 s, 63°C for 45 s, 72°C for 1 min; 72°C for 10 min; 4°C for 10 min. The correct amplification was confirmed by Sanger sequencing (Eurofins). Amplicons were purified with the Wizard Gel and PCR Clean-up Kit (Promega) before library preparation. The PCR amplicon was barcoded with the UDP Index set (Illumina). We performed 11 cycles of PCR with the HiFi Kapa amplification kit (Roche). The amplicons were successively purified with Ampure beads (Beckman Coulter) and run onto a DNA 1000 ScreenTape (Tapestation 4200, Agilent). Libraries were appropriately diluted, mixed with 50% PhiX, and sequenced on a MiSeq v.2 300 in paired-end mode. We expected around 1-2 M clusters for each sample. Demultiplexing was performed with the Bcl2Fastq algorithm.

Paired-end sequencing reads were quality-controlled through FastQC (v.0.12.1) before and after primer trimming performed with Cutadapt (v.5.1). Forward and reverse primer sequences were identified at the 5′ end of R1 and R2 reads, respectively, with a minimum overlap of 12 nucleotides, an error rate of 0.15, and indel-free matching. Any sequence upstream of the primer was removed while the primer itself was retained in the read. Read pairs in which either primer was not detected were discarded.

To evaluate the genome editing results, we used the CRISPResso2 pipeline (https://github.com/pinellolab/CRISPResso2).[58] Batch processing was conducted to allow high-throughput evaluation on multiple datasets. Analyses were performed through the NHEJ mode, which quantifies insertions, deletions, and substitutions introduced at the target site because of the error-prone DNA repair process following the induction of DSBs.

#### IHC analysis and quantification of $GFAP^+$ areas and RF distribution

The brain hemisphere was collected and fixed in buffered 10% formalin. It was trimmed into cranio-caudal transverse sections following published guidelines[87] and embedded in paraffin. Sequential sections measuring 3–4 μm in thickness were cut, up to a maximum of 25 sections. The similarity of anterior-posterior coordinates was confirmed in hematoxylin and eosin (H&E) stained sections. H&E staining was conducted according to standard protocols through an automated stainer (Bio-Optica, model #05–06002, Mayer's Hematoxylin, and Eosin from Bio-Optica, #05–10002).

For IHC analysis, slides were immunostained with the Automatic Leica BOND RX system (Leica Microsystems GmbH, Wetzlar, Germany). First, tissues were deparaffinized and pre-treated with Epitope Retrieval Solution1 (ER1 Citrate Buffer) at 100°C for 20 min. Primary antibodies (GFAP, SySy, 1:1000) were developed by using Bond Polymer Refine Detection (Leica, DS9800). The slides were then digitized with an Aperio AT2 scanner at a magnification of 20× (Leica Biosystems) and visualized with Aperio ImageScope software (v.12.4.6.5003, Leica).

IHC signal was analyzed with ImageJ software. The $GFAP^+$ pixel area was quantified by separating the different color channels of the image with the Color Deconvolution tool (H DAB option) and measuring the $GFAP^+$ area in channel 2, using a previously optimized threshold of 150. The resulting pixel area was expressed as the percentage of the total slice pixel area. WM regions were selected within whole slices on the basis of anatomical landmarks (Figure S6).

RFs were identified as amorphous eosinophilic aggregates located close to nuclei. RFs were manually quantified in H&E-processed sections. Images of the corpus callosum and the periventricular area were captured at 20× magnification with an Eclipse Ni microscope (Nikon). A minimum of 7 images per section and 3 sections per animal were analyzed, resulting in 43–656 RFs counted in each section. The image analysis was conducted with ImageJ software. The investigators performed imaging and analysis blind to the experimental conditions. An operator not involved in the analysis renamed the images for the quantification of RF and $GFAP^+$ areas with neutral alphanumeric codes. A second operator performed all quantifications with only anonymized files, and the first operator later reassigned the analyzed data to the correct experimental groups.

#### AAV integration SLiM-PCR and RAAVioli pipeline

AAV ISs were profiled through SLiM-PCR.[88,89] Genomic DNA was fragmented to ∼1,000 bp through a Covaris E220 Ultrasonicator (Covaris Inc.) and processed with the NEBNext UltraII DNA Library Prep Kit (New England Biolabs) for end-repair, 3′-adenylation, and ligation to custom linker cassettes (LCs; Integrated DNA Technologies), which contained unique 8-nt barcodes for sample identification. Ligation products were amplified by 25-cycle exponential PCR with primers specific to AAV and LC regions (see Table S7 for primer and linker sequences). Technical replicates ($n = 3$) were performed with 10 ng of input DNA. A nested PCR (10 cycles) fused Illumina adapters and an additional barcode. Products were quantified with the KAPA Library Quantification Kit (Kapa Biosystems) and sequenced on the Illumina NovaSeq platform.

For the identification of AAV IS, we used the bioinformatic pipeline named RAAVioli.[61] Briefly, raw sequencing reads were trimmed for

Please cite this article in press as: Hillen et al., Targeting white matter astrocytes with a *Gfap*-disruptive Cas9 nuclease benefits a murine model of Alexander disease, Molecular Therapy (2026), https://doi.org/10.1016/j.ymthe.2026.09.019



adapters and low-quality bases (FastQC, Flexbar, Trimmomatic), and vector-derived sequences were identified by alignment to the AAV reference genome (BWA-MEM). Reads containing expected AAV termini were then mapped to a hybrid mouse and vector genomes (mm9+ AAV). Integration junctions were identified with a custom Python pipeline that parsed CIGAR strings to classify junctions into: (1) blunt ends, (2) microhomology-mediated joins, and (3) insertions. Unique ISs were defined by junction position and AAV rearrangements, with a ±10 bp window and requiring ≥3 independent sheared DNA fragments. Clonal abundance was estimated by counting distinct shear sites associated with each IS, serving as a proxy for originating cell numbers and minimizing PCR bias. After mapping, the AAV ISs were annotated on the mm10 mouse genome version with the liftOver tool.

### Statistics

In *in vitro* assays, technical replicates were included in each independent experiment, and at least $n = 2–3$ independent repetitions were conducted for each experiment. The sample size of *in vivo* treatment groups was determined by using a power analysis on the basis of G*power v.3.1.9.6 (effect size f = 0.7; power = 0.9; α err prob = 0.05). The study included $n = 9$ animals per group. All samples reported in this study reflect biological replicates. Littermates of either sex were randomly allocated to experimental conditions as permitted by genotype.

Data analysis was performed with GraphPad Prism for Windows (v.10.2.3), and data are shown as mean with standard deviation, except as stated otherwise in the figure legends. All data were assessed for normality by Shapiro-Wilk tests and tested with parametric (Student *t* test or ANOVA) or non-parametric (Mann-Whitney U or Kruskal-Wallis) tests accordingly. Tukey's B method was used for post hoc testing. Correlation analysis was performed with Spearman's correlation. Statistical tests and the number of samples are indicated in the manuscript and figure legends. No samples or data collected in the correct experimental conditions were excluded from the analysis. Data were analyzed in a blinded manner.

## DATA AND CODE AVAILABILITY

Data are available within the published article and supplemental information. Additional data are available from the corresponding author on reasonable request.

## ACKNOWLEDGMENTS

We thank Serena Gallorini and Davide Sala for helping with injection procedures and sample collection and Amleto Fiocchi for support in IHC analysis. Part of this work was carried out in the core facilities established at IRCSS Ospedale San Raffaele and Vita-Salute San Raffaele University, Animal Histopathology Facility, ALEMBIC (Advanced Light and Electron Microscopy BioImaging Center), COSR (Center for Omics Sciences), and FRACTAL (Flow cytometry Resource, Advanced Cytometry Technical Applications Laboratory). Funding agencies: Unione Europea - Next Generation EU, Missione 4, Componente 1, CUP D43C22004340006 (to V.M.); Horizon 2020 Research and Innovation Programme, Marie Sklodowska-Curie, grant agreement no. 895111 (to V.M.); European Commission (Horizon Europe), EUROPEAN RARE DISEASES RESEARCH ALLIANCE (ERDERA), grant agreement no. 101156595 (to V.M.); EndAxD - End Alexander Disease Foundation, grant agreement ID: 2025 EndAxD Grant Program (to V.M.); European Leukodystrophy Association, grant agreement no. 2020-010I2 (to A.G.); European Leukodystrophy Association, grant agreement no. 2022-009C2 (to A.G. and E.M.); European Leukodystrophy Association, grant agreement no. 2021-019I1 (to E.M.); Telethon Foundation grants, grant agreement nos. TGT16D02 and TTAGD0222TT (to A.G.); Telethon Foundation grants, grant agreement nos. TGT11D1, TGT16B01, and TGT16B03 (to E.M.); and PNRR-National Center for Gene Therapy and Drugs Based on RNA Technology - project #CN00000041; B83C22002860006 (to V.B.). Sponsor(s) had no role in the study design, collection, analysis, and interpretation of data or in submitting the article for publication.

## AUTHOR CONTRIBUTIONS

V.M. and A.E.J.H. designed and conceived the study. A.E.J.H. and I.C. performed *in vitro* and *in vivo* experiments. I.L. and G.Z. performed *in vitro* experiments. B.G., F.B., and S.A. performed AAV integration studies. G.S. analyzed deep-sequencing data. A.L. and F.G. performed long-range SLiM-PCR. E.M. provided expertise and resources for conducting AAV integration studies and deep-sequencing analysis. M.M. and M.R. performed GUIDE-seq analysis and deep-sequencing of off-targets, under the supervision of M.A. R.N. performed histopathological and IHC analyses, under the supervision of F.S. S.G.G. produced AAV vectors under the supervision of V.B. V.M. and A.G. provided expertise and resources and supervised the whole study. V.M. and A.E.J.H. wrote the manuscript, with input from A.G.

## DECLARATION OF INTERESTS

The authors declare no conflict of interest.

## SUPPLEMENTAL INFORMATION

Supplemental information can be found online at https://doi.org/10.1016/j.ymthe.2026.09.019.

## REFERENCES

1. Zhou, B., Zuo, Y.X., and Jiang, R.T. (2019). Astrocyte morphology: Diversity, plasticity, and role in neurological diseases. CNS Neurosci. Ther. *25*, 665–673. https://doi.org/10.1111/cns.13123.

2. Kıray, H., Lindsay, S.L., Hosseinzadeh, S., and Barnett, S.C. (2016). The multifaceted role of astrocytes in regulating myelination. Exp. Neurol. *283*, 541–549. https://doi.org/10.1016/j.expneurol.2016.03.009.

3. Sofroniew, M.V., and Vinters, H.V. (2010). Astrocytes: Biology and pathology. Acta Neuropathol. *119*, 7–35. https://doi.org/10.1007/s00401-009-0619-8.

4. Kimelberg, H.K., and Nedergaard, M. (2010). Functions of Astrocytes and their Potential As Therapeutic Targets. Neurotherapeutics *7*, 338–353. https://doi.org/10.1016/j.nurt.2010.07.006.

5. Valori, C.F., Guidotti, G., Brambilla, L., and Rossi, D. (2019). Astrocytes: Emerging Therapeutic Targets in Neurological Disorders. Trends Mol. Med. *25*, 750–759. https://doi.org/10.1016/j.molmed.2019.04.010.

6. Messing, A., Brenner, M., Feany, M.B., Nedergaard, M., and Goldman, J.E. (2012). Alexander Disease. J. Neurosci. *32*, 5017–5023. https://doi.org/10.1523/JNEUROSCI.5384-11.2012.

7. Hol, E.M., and Pekny, M. (2015). Glial fibrillary acidic protein (GFAP) and the astrocyte intermediate filament system in diseases of the central nervous system. Curr. Opin. Cell Biol. *32*, 121–130. https://doi.org/10.1016/j.ceb.2015.02.004.

8. Messing, A., LaPash Daniels, C.M., and Hagemann, T.L. (2010). Strategies for Treatment in Alexander Disease. Neurotherapeutics *7*, 507–515. https://doi.org/10.1016/j.nurt.2010.05.013.

9. Bachetti, T., Vaia, Y., Grossi, A., Rosamilia, F., Bertini, E., Nicita, F., Bellitto, D., Eichler, F., Bernard, G., Nagy, A., et al. (2026). Genotype-phenotype correlations of GFAP variants in type I Alexander disease subtypes. Mol. Genet. Metab. *147*, 109689. https://doi.org/10.1016/j.ymgme.2025.109689.

10. Yoshida, T. (2020). Clinical characteristics of Alexander disease. Neurodegener. Dis. Manag. *10*, 325–333. https://doi.org/10.2217/nmt-2020-0022.

11. Heaven, M.R., Flint, D., Randall, S.M., Sosunov, A.A., Wilson, L., Barnes, S., Goldman, J.E., Muddiman, D.C., and Brenner, M. (2016). Composition of Rosenthal Fibers, the Protein Aggregate Hallmark of Alexander Disease. J. Proteome Res. *15*, 2265–2282. https://doi.org/10.1021/acs.jproteome.6b00316.

12. Messing, A. (2019). Refining the concept of GFAP toxicity in Alexander disease. J. Neurodev. Disord. *11*, 27. https://doi.org/10.1186/s11689-019-9290-0.

13. Jany, P.L., Agosta, G.E., Benko, W.S., Eickhoff, J.C., Keller, S.R., Köehler, W., Koeller, D., Mar, S., Naidu, S., Marie Ness, J., et al. (2015). CSF and blood levels of GFAP in Alexander disease. eNeuro *2*, 1–11. https://doi.org/10.1523/ENEURO.0080-15.2015.

14. Ashton, N.J., Di Molfetta, G., Tan, K., Blennow, K., Zetterberg, H., and Messing, A. (2024). Plasma concentrations of glial fibrillary acidic protein, neurofilament light, and tau in Alexander disease. Neurol. Sci. *45*, 4513–4518. https://doi.org/10.1007/s10072-024-07495-8.

15. Waldman, A.T., Takanohashi, A., Joung, J.Y., Liu, G.W., Arnold, K., Pizzino, A., Faig, W., Woidill, S., Narula, S., and Vanderver, A.L. (2026). Characterization of Clinical Phenotype to Glial Fibrillary Acidic Protein Concentrations in Alexander Disease. Ann. Clin. Transl. Neurol. *13*, 1206–1221. https://doi.org/10.1002/acn3.70305.

16. Hagemann, T.L. (2022). Alexander disease: models, mechanisms, and medicine. Curr. Opin. Neurobiol. *72*, 140–147. https://doi.org/10.1016/j.conb.2021.10.002.

17. Heaven, M.R., Herren, A.W., Flint, D.L., Pacheco, N.L., Li, J., Tang, A., Khan, F., Goldman, J.E., Phinney, B.S., and Olsen, M.L. (2022). Metabolic Enzyme Alterations and Astrocyte Dysfunction in a Murine Model of Alexander Disease With Severe Reactive Gliosis. Mol. Cell. Proteomics *21*, 100180. https://doi.org/10.1016/j.mcpro.2021.100180.

18. Wang, L., Bukhari, H., Kong, L., Hagemann, T.L., Zhang, S.-C., Messing, A., and Feany, M.B. (2022). Anastasis Drives Senescence and Non-Cell Autonomous Neurodegeneration in the Astrogliopathy Alexander Disease. J. Neurosci. *42*, 2584–2597. https://doi.org/10.1523/JNEUROSCI.1659-21.2021.

19. Bellitto, D., Bozzo, M., Ravera, S., Bertola, N., Rosamilia, F., Milia, J., Barboro, P., Vargas, G.C., Di Lisa, D., Pastorino, L., et al. (2025). A multi-omics approach reveals impaired lipid metabolism and oxidative stress in a zebrafish model of Alexander disease. Redox Biol. *81*, 103544. https://doi.org/10.1016/j.redox.2025.103544.

20. Viedma-Poyatos, Á., González-Jiménez, P., Pajares, M.A., and Pérez-Sala, D. (2022). Alexander disease GFAP R239C mutant shows increased susceptibility to lipoxidation and elicits mitochondrial dysfunction and oxidative stress. Redox Biol. *55*, 102415. https://doi.org/10.1016/j.redox.2022.102415.

21. Hagemann, T.L., Jobe, E.M., and Messing, A. (2012). Genetic ablation of Nrf2/antioxidant response pathway in alexander disease mice reduces hippocampal gliosis but does not impact survival. PLoS One *7*, e37304. https://doi.org/10.1371/journal.pone.0037304.

22. Wang, L., Hagemann, T.L., Kalwa, H., Michel, T., Messing, A., and Feany, M.B. (2015). Nitric oxide mediates glial-induced neurodegeneration in Alexander disease. Nat. Commun. *6*, 8966. https://doi.org/10.1038/ncomms9966.

23. Matejuk, A., and Ransohoff, R.M. (2020). Crosstalk Between Astrocytes and Microglia: An Overview. Front. Immunol. *11*, 1416. https://doi.org/10.3389/fimmu.2020.01416.

24. Lee, H.G., Lee, J.H., Flausino, L.E., and Quintana, F.J. (2023). Neuroinflammation: An astrocyte perspective. Sci. Transl. Med. *15*, eadi7828. https://doi.org/10.1126/scitranslmed.adi7828.

25. Li, L., Tian, E., Chen, X., Chao, J., Klein, J., Qu, Q., Sun, G., Sun, G., Huang, Y., Warden, C.D., et al. (2018). GFAP Mutations in Astrocytes Impair Oligodendrocyte Progenitor Proliferation and Myelination in an hiPSC Model of Alexander Disease. Cell Stem Cell *23*, 239–251.e6. https://doi.org/10.1016/j.stem.2018.07.009.

26. Van der Knaap, M.S., Naidu, S., Breiter, S.N., Blaser, S., Stroink, H., Springer, S., Begeer, J.C., Van Coster, R., Barth, P.G., Thomas, N.H., et al. (2001). Alexander disease: Diagnosis with MR imaging. AJNR. Am. J. Neuroradiol. *22*, 541–552.

27. Yoshida, T., Sasaki, M., Yoshida, M., Namekawa, M., Okamoto, Y., Tsujino, S., Sasayama, H., Mizuta, I., and Nakagawa, M.; Alexander Disease Study Group in Japan (2011). Nationwide survey of Alexander disease in Japan and proposed new guidelines for diagnosis. J. Neurol. *258*, 1998–2008. https://doi.org/10.1007/s00415-011-6056-3.

28. Vaia, Y., Mura, E., and Tonduti, D. (2023). Type I Alexander disease: Update and validation of the clinical evolution-based classification. Mol. Genet. Metab. *138*, 107540. https://doi.org/10.1016/j.ymgme.2023.107540.

29. Prust, M., Wang, J., Morizono, H., Messing, A., Brenner, M., Gordon, E., Hartka, T., Sokohl, A., Schiffmann, R., Gordish-Dressman, H., et al. (2011). GFAP mutations, age at onset, and clinical subtypes in Alexander disease. Neurology *77*, 1287–1294. https://doi.org/10.1212/WNL.0b013e3182309f72.

30. Grossi, A., Rosamilia, F., Carestiato, S., Salsano, E., Ceccherini, I., and Bachetti, T. (2024). A systematic review and meta-analysis of GFAP gene variants in Alexander disease. Sci. Rep. *14*, 24341. https://doi.org/10.1038/s41598-024-75383-4.

31. Messing, A., Waldman, A.T., and Bolt, D.M. (2025). Genotype-Phenotype Association for 14 GFAP Variants in Alexander Disease. Neurol. Genet. *11*, e200270. https://doi.org/10.1212/NXG.0000000000200270.

32. Hagemann, T.L., Powers, B., Mazur, C., Kim, A., Wheeler, S., Hung, G., Swayze, E., and Messing, A. (2018). Antisense suppression of glial fibrillary acidic protein as a treatment for Alexander disease. Ann. Neurol. *83*, 27–39. https://doi.org/10.1002/ana.25118.

33. Hagemann, T.L., Powers, B., Lin, N.-H., Mohamed, A.F., Dague, K.L., Hannah, S.C., Bachmann, G., Mazur, C., Rigo, F., Olsen, A.L., et al. (2021). Antisense therapy in a rat model of Alexander disease reverses GFAP pathology, white matter deficits, and motor impairment. Sci. Transl. Med. *13*, eabg4711. https://doi.org/10.1126/scitranslmed.abg4711.

34. Messing, A., and Brenner, M. (2020). GFAP at 50. ASN Neuro *12*, 1759091420949680. https://doi.org/10.1177/1759091420949680.

35. Brenner, M. (2014). Role of GFAP in CNS injuries. Neurosci. Lett. *565*, 7–13. https://doi.org/10.1016/j.neulet.2014.01.055.

36. Ginn, S.L., Mandwie, M., Alexander, I.E., Edelstein, M., and Abedi, M.R. (2024). Gene therapy clinical trials worldwide to 2023-an update. J. Gene Med. *26*, e3721. https://doi.org/10.1002/jgm.3721.

37. Gillmore, J.D., Gane, E., Taubel, J., Kao, J., Fontana, M., Maitland, M.L., Seitzer, J., O'Connell, D., Walsh, K.R., Wood, K., et al. (2021). CRISPR-Cas9 In Vivo Gene Editing for Transthyretin Amyloidosis. N. Engl. J. Med. *385*, 493–502. https://doi.org/10.1056/nejmoa2107454.

38. Pierce, E.A., Aleman, T.S., Jayasundera, K.T., Ashimatey, B.S., Kim, K., Rashid, A., Jaskolka, M.C., Myers, R.L., Lam, B.L., Bailey, S.T., et al. (2024). Gene Editing for CEP290 -Associated Retinal Degeneration. N. Engl. J. Med. *390*, 1972–1984. https://doi.org/10.1056/nejmoa2309915.

39. Torregrosa, T., Lehman, S., Hana, S., Marsh, G., Xu, S., Koszka, K., Mastrangelo, N., McCampbell, A., Henderson, C.E., and Lo, S.C. (2021). Use of CRISPR/Cas9-mediated disruption of CNS cell type genes to profile transduction of AAV by neonatal intracerebroventricular delivery in mice. Gene Ther. *28*, 456–468. https://doi.org/10.1038/s41434-021-00223-3.

40. Park, H., Oh, J., Shim, G., Cho, B., Chang, Y., Kim, S., Baek, S., Kim, H., Shin, J., Choi, H., et al. (2019). In vivo neuronal gene editing via CRISPR–Cas9 amphiphilic nanocomplexes alleviates deficits in mouse models of Alzheimer's disease. Nat. Neurosci. *22*, 524–528. https://doi.org/10.1038/s41593-019-0352-0.

41. Ekman, F.K., Ojala, D.S., Adil, M.M., Lopez, P.A., Schaffer, D.V., and Gaj, T. (2019). CRISPR-Cas9-Mediated Genome Editing Increases Lifespan and Improves Motor Deficits in a Huntington's Disease Mouse Model. Mol. Ther. Nucleic Acids *17*, 829–839. https://doi.org/10.1016/j.omtn.2019.07.009.

42. Laurent, M., Geoffroy, M., Pavani, G., and Guiraud, S. (2024). CRISPR-Based Gene Therapies: From Preclinical to Clinical Treatments. Cells *13*, 800. https://doi.org/10.3390/cells13100800.

43. Nishimasu, H., Cong, L., Yan, W.X., Ran, F.A., Zetsche, B., Li, Y., Kurabayashi, A., Ishitani, R., Zhang, F., and Nureki, O. (2015). Crystal Structure of Staphylococcus aureus Cas9. Cell *162*, 1113–1126. https://doi.org/10.1016/j.cell.2015.08.007.

44. Ran, F.A., Cong, L., Yan, W.X., Scott, D.A., Gootenberg, J.S., Kriz, A.J., Zetsche, B., Shalem, O., Wu, X., Makarova, K.S., et al. (2015). In vivo genome editing using Staphylococcus aureus Cas9. Nature *520*, 186–191. https://doi.org/10.1038/nature14299.

45. Meneghini, V., Peviani, M., Luciani, M., Zambonini, G., and Gritti, A. (2021). Delivery Platforms for CRISPR/Cas9 Genome Editing of Glial Cells in the Central Nervous System. Front. Genome *3*, 644319. https://doi.org/10.3389/fgeed.2021.644319.

46. Kang, L., Jin, S., Wang, J., Lv, Z., Xin, C., Tan, C., Zhao, M., Wang, L., and Liu, J. (2023). AAV vectors applied to the treatment of CNS disorders: Clinical status

Please cite this article in press as: Hillen et al., Targeting white matter astrocytes with a *Gfap*-disruptive Cas9 nuclease benefits a murine model of Alexander disease, Molecular Therapy (2026), https://doi.org/10.1016/j.ymthe.2026.09.019



and challenges. J. Control Release *355*, 458–473. https://doi.org/10.1016/j.jconrel.2023.01.067.

47. Wang, J.H., Gessler, D.J., Zhan, W., Gallagher, T.L., and Gao, G. (2024). Adeno-associated virus as a delivery vector for gene therapy of human diseases. Signal Transduct. Target. Ther. *9*, 78. https://doi.org/10.1038/s41392-024-01780-w.

48. Simpson, B.P., Yrigollen, C.M., Izda, A., and Davidson, B.L. (2023). Targeted long-read sequencing captures CRISPR editing and AAV integration outcomes in brain. Mol. Ther. *31*, 760–773. https://doi.org/10.1016/j.ymthe.2023.01.004.

49. Hanlon, K.S., Kleinstiver, B.P., Garcia, S.P., Zaborowski, M.P., Volak, A., Spirig, S.E., Muller, A., Sousa, A.A., Tsai, S.Q., Bengtsson, N.E., et al. (2019). High levels of AAV vector integration into CRISPR-induced DNA breaks. Nat. Commun. *10*, 4439. https://doi.org/10.1038/s41467-019-12449-2.

50. Bazick, H.O., Mao, H., Niehaus, J.K., Wolter, J.M., and Zylka, M.J. (2024). AAV vector-derived elements integrate into Cas9-generated double-strand breaks and disrupt gene transcription. Mol. Ther. *32*, 4122–4137. https://doi.org/10.1016/j.ymthe.2024.09.032.

51. Hagemann, T.L., Connor, J.X., and Messing, A. (2006). Alexander Disease-Associated Glial Fibrillary Acidic Protein Mutations in Mice Induce Rosenthal Fiber Formation and a White Matter Stress Response. J. Neurosci. *26*, 11162–11173. https://doi.org/10.1523/JNEUROSCI.3260-06.2006.

52. Brinkman, E.K., Chen, T., Amendola, M., and Van Steensel, B. (2014). Easy quantitative assessment of genome editing by sequence trace decomposition. Nucleic Acids Res. *42*, e168. https://doi.org/10.1093/nar/gku936.

53. Olabarria, M., Putilina, M., Riemer, E.C., and Goldman, J.E. (2015). Astrocyte pathology in Alexander disease causes a marked inflammatory environment. Acta Neuropathol. *130*, 469–486. https://doi.org/10.1007/s00401-015-1469-1.

54. Sosunov, A., Olabarria, M., and Goldman, J.E. (2018). Alexander disease: an astrocytopathy that produces a leukodystrophy. Brain Pathol. *28*, 388–398. https://doi.org/10.1111/bpa.12601.

55. Hammond, S.L., Leek, A.N., Richman, E.H., and Tjalkens, R.B. (2017). Cellular selectivity of AAV serotypes for gene delivery in neurons and astrocytes by neonatal intracerebroventricular injection. PLoS One *12*, e0188830. https://doi.org/10.1371/journal.pone.0188830.

56. Reemst, K., Noctor, S.C., Lucassen, P.J., and Hol, E.M. (2016). The indispensable roles of microglia and astrocytes during brain development. Front. Hum. Neurosci. *10*, 566. https://doi.org/10.3389/fnhum.2016.00566.

57. Lee, Y., Messing, A., Su, M., and Brenner, M. (2008). GFAP promoter elements required for region-specific and astrocyte-specific expression. Glia *56*, 481–493. https://doi.org/10.1002/glia.20622.

58. Clement, K., Rees, H., Canver, M.C., Gehrke, J.M., Farouni, R., Hsu, J.Y., Cole, M.A., Liu, D.R., Joung, J.K., Bauer, D.E., and Pinello, L. (2019). CRISPResso2 provides accurate and rapid genome editing sequence analysis. Nat. Biotechnol. *37*, 224–226. https://doi.org/10.1038/s41587-019-0032-3.

59. Boyd, M.M., Litscher, S.J., Seitz, L.L., Messing, A., Hagemann, T.L., and Collier, L.S. (2021). Pexidartinib treatment in Alexander disease model mice reduces macrophage numbers and increases glial fibrillary acidic protein levels, yet has minimal impact on other disease phenotypes. J. Neuroinflammation *18*, 67. https://doi.org/10.1186/s12974-021-02118-x.

60. Calabria, A., Cipriani, C., Spinozzi, G., Rudilosso, L., Esposito, S., Benedicenti, F., Albertini, A., Pouzolles, M., Luoni, M., Giannelli, S., et al. (2023). Intrathymic AAV delivery results in therapeutic site-specific integration at TCR loci. Blood *141*, 2316–2329. https://doi.org/10.1182/blood.2022017378.

61. Ferrari, S., Jacob, A., Cesana, D., Laugel, M., Beretta, S., Varesi, A., Unali, G., Conti, A., Canarutto, D., Albano, L., et al. (2022). Choice of template delivery mitigates the genotoxic risk and adverse impact of editing in human hematopoietic stem cells. Cell Stem Cell *29*, 1428–1444.e9. https://doi.org/10.1016/j.stem.2022.09.001.

62. McGinnis, J.P., Ortiz-Guzman, J., Guevara, M.C., Mallannagari, S., Belfort, B.D.W., Bao, S., Srivastava, S., Morkas, M., Ji, E., Addison, A., et al. (2025). Common AAV gene therapy vectors show nonselective transduction of ex vivo human brain tissue. Mol. Ther. Methods Clin. Dev. *33*, 101494. https://doi.org/10.1016/j.omtm.2025.101494.

63. Chakrabarty, P., Rosario, A., Cruz, P., Siemienski, Z., Ceballos-Diaz, C., Crosby, K., Jansen, K., Borchelt, D.R., Kim, J.Y., Jankowsky, J.L., et al. (2013). Capsid Serotype and Timing of Injection Determines AAV Transduction in the Neonatal Mice Brain. PLoS One *8*, e67680. https://doi.org/10.1371/journal.pone.0067680.

64. Degl'Innocenti, E., and Dell'Anno, M.T. (2023). Human and mouse cortical astrocytes: a comparative view from development to morphological and functional characterization. Front. Neuroanat. *17*, 1130729. https://doi.org/10.3389/fnana.2023.1130729.

65. Zhou, L., Wang, Y., Xu, Y., Zhang, Y., and Zhu, C. (2024). Advances in AAV-mediated gene replacement therapy for pediatric monogenic neurological disorders. Mol. Ther. Methods Clin. Dev. *32*, 101357. https://doi.org/10.1016/j.omtm.2024.101357.

66. Cain, J.T., Likhite, S., White, K.A., Timm, D.J., Davis, S.S., Johnson, T.B., Dennys-Rivers, C.N., Rinaldi, F., Motti, D., Corcoran, S., et al. (2019). Gene Therapy Corrects Brain and Behavioral Pathologies in CLN6-Batten Disease. Mol. Ther. *27*, 1836–1847. https://doi.org/10.1016/j.ymthe.2019.06.015.

67. Galvan, A., Petkau, T.L., Hill, A.M., Korecki, A.J., Lu, G., Choi, D., Rahman, K., Simpson, E.M., Leavitt, B.R., and Smith, Y. (2021). Intracerebroventricular Administration of AAV9-PHP.B SYN1-EmGFP Induces Widespread Transgene Expression in the Mouse and Monkey Central Nervous System. Hum. Gene Ther. *32*, 599–615. https://doi.org/10.1089/hum.2020.301.

68. Davis, J.R., Wang, X., Witte, I.P., Huang, T.P., Levy, J.M., Raguram, A., Banskota, S., Seidah, N.G., Musunuru, K., and Liu, D.R. (2022). Efficient in vivo base editing via single adeno-associated viruses with size-optimized genomes encoding compact adenine base editors. Nat. Biomed. Eng. *6*, 1272–1283. https://doi.org/10.1038/s41551-022-00911-4.

69. Gleichman, A.J., Kawaguchi, R., Sofroniew, M.V., and Carmichael, S.T. (2023). A toolbox of astrocyte-specific, serotype-independent adeno-associated viral vectors using microRNA targeting sequences. Nat. Commun. *14*, 7426. https://doi.org/10.1038/s41467-023-42746-w.

70. Lattanzi, A., Salvagno, C., Maderna, C., Benedicenti, F., Morena, F., Kulik, W., Naldini, L., Montini, E., Martino, S., and Gritti, A. (2014). Therapeutic benefit of lentiviral-mediated neonatal intracerebral gene therapy in a mouse model of globoid cell leukodystrophy. Hum. Mol. Genet. *23*, 3250–3268. https://doi.org/10.1093/hmg/ddu034.

71. Moody, L.R., Barrett-Wilt, G.A., Sussman, M.R., and Messing, A. (2017). Glial fibrillary acidic protein exhibits altered turnover kinetics in a mouse model of alexander disease. J. Biol. Chem. *292*, 5814–5824. https://doi.org/10.1074/jbc.M116.772020.

72. McCall, M.A., Gregg, R.G., Behringer, R.R., Brenner, M., Delaney, C.L., Galbreath, E.J., Zhang, C.L., Pearce, R.A., Chiu, S.Y., and Messing, A. (1996). Targeted deletion in astrocyte intermediate filament (Gfap) alters neuronal physiology. Proc. Natl. Acad. Sci. USA *93*, 6361–6366. https://doi.org/10.1073/pnas.93.13.6361.

73. Nawashiro, H., Brenner, M., Fukui, S., Shima, K., and Hallenbeck, J.M. (2000). High Susceptibility to Cerebral Ischemia in GFAP-Null Mice. J. Cereb. Blood Flow Metab. *20*, 1040–1044. https://doi.org/10.1097/00004647-200007000-00003.

74. Nawashiro, H., Messing, A., Azzam, N., and Brenner, M. (1998). Mice lacking GFAP are hypersensitive to traumatic cerebrospinal injury. Neuroreport *9*, 1691–1696. https://doi.org/10.1097/00001756-199806010-00004.

75. Messing, A., Head, M.W., Galles, K., Galbreath, E.J., Goldman, J.E., and Brenner, M. (1998). Fatal encephalopathy with astrocyte inclusions in GFAP transgenic mice. Am. J. Pathol. *152*, 391–398.

76. Tang, G., Xu, Z., and Goldman, J.E. (2006). Synergistic effects of the SAPK/JNK and the proteasome pathway on glial fibrillary acidic protein (GFAP) accumulation in Alexander disease. J. Biol. Chem. *281*, 38634–38643. https://doi.org/10.1074/jbc.M604942200.

77. Bi, F., Huang, C., Tong, J., Qiu, G., Huang, B., Wu, Q., Li, F., Xu, Z., Bowser, R., Xia, X.G., and Zhou, H. (2013). Reactive astrocytes secrete lcn2 to promote neuron death. Proc. Natl. Acad. Sci. USA *110*, 4069–4074. https://doi.org/10.1073/pnas.1218497110.

78. Schmidheini, L., Mathis, N., Marquart, K.F., Rothgangl, T., Kissling, L., Böck, D., Chanez, C., Wang, J.P., Jinek, M., and Schwank, G. (2024). Continuous directed evolution of a compact CjCas9 variant with broad PAM compatibility. Nat. Chem. Biol. *20*, 333–343. https://doi.org/10.1038/s41589-023-01427-x.

79. Zhang, H., Bamidele, N., Liu, P., Ojelabi, O., Gao, X.D., Rodriguez, T., Cheng, H., Kelly, K., Watts, J.K., Xie, J., et al. (2022). Adenine Base Editing In Vivo with a

Single Adeno-Associated Virus Vector. GEN. Biotechnol. *1*, 285–299. https://doi.org/10.1089/genbio.2022.0015.

80. Nguyen Tran, M.T., Mohd Khalid, M.K.N., Wang, Q., Walker, J.K.R., Lidgerwood, G.E., Dilworth, K.L., Lisowski, L., Pébay, A., and Hewitt, A.W. (2020). Engineering domain-inlaid SaCas9 adenine base editors with reduced RNA off-targets and increased on-target DNA editing. Nat. Commun. *11*, 4871. https://doi.org/10.1038/s41467-020-18715-y.

81. Pedrazzoli, E., Demozzi, M., Visentin, E., Ciciani, M., Bonuzzi, I., Pezzè, L., Lucchetta, L., Maule, G., Amistadi, S., Esposito, F., et al. (2024). CoCas9 is a compact nuclease from the human microbiome for efficient and precise genome editing. Nat. Commun. *15*, 3478. https://doi.org/10.1038/s41467-024-47800-9.

82. Ruta, G.V., Ciciani, M., Kheir, E., Gentile, M.D., Amistadi, S., Casini, A., and Cereseto, A. (2024). Eukaryotic-driven directed evolution of Cas9 nucleases. Genome Biol. *25*, 79. https://doi.org/10.1186/s13059-024-03215-9.

83. Chen, S., Liu, Z., Xie, W., Yu, H., Lai, L., and Li, Z. (2022). Compact Cje3Cas9 for Efficient in Vivo Genome Editing and Adenine Base Editing. CRISPR J. *5*, 472–486. https://doi.org/10.1089/crispr.2021.0143.

84. Fumagalli, F., Calbi, V., Gallo, V., Zambon, A.A., Recupero, S., Ciotti, F., Sarzana, M., Fraschini, M., Scarparo, S., De Mattia, F., et al. (2025). Long-Term Effects of Atidarsagene Autotemcel for Metachromatic Leukodystrophy. N. Engl. J. Med. *392*, 1609–1620. https://doi.org/10.1056/nejmoa2405727.

85. Mura, E., Nicita, F., Masnada, S., Battini, R., Ticci, C., Montomoli, M., Berardinelli, A., Pantaleoni, C., Ardissone, A., Foiadelli, T., et al. (2021). Alexander disease evolution over time: data from an Italian cohort of pediatric-onset patients. Mol. Genet. Metab. *134*, 353–358. https://doi.org/10.1016/j.ymgme.2021.11.009.

86. Kim, J.Y., Grunke, S.D., Levites, Y., Golde, T.E., and Jankowsky, J.L. (2014). Intracerebroventricular viral injection of the neonatal mouse brain for persistent and widespread neuronal transduction. J. Vis. Exp. *15*, 51863. https://doi.org/10.3791/51863.

87. Morawietz, G., Ruehl-Fehlert, C., Kittel, B., Bube, A., Keane, K., Halm, S., Heuser, A., and Hellmann, J.; RITA Group; NACAD Group (2004). Revised guides for organ sampling and trimming in rats and mice – Part 3. A joint publication of the RITA and NACAD groups. Exp. Toxicol. Pathol. *55*, 433–449. https://doi.org/10.1078/0940-2993-00350.

88. Cesana, D., Calabria, A., Rudilosso, L., Gallina, P., Benedicenti, F., Spinozzi, G., Schiroli, G., Magnani, A., Acquati, S., Fumagalli, F., et al. (2021). Retrieval of vector integration sites from cell-free DNA. Nat. Med. *27*, 1458–1470. https://doi.org/10.1038/s41591-021-01389-4.

89. Chiu, J., March, P.E., Lee, R., and Tillett, D. (2004). Site-directed, Ligase-Independent Mutagenesis (SLIM): a single-tube methodology approaching 100% efficiency in 4 h. Nucleic Acids Res. *32*, e174. https://doi.org/10.1093/nar/gnh172.